Transcriptomic comparison of two selective retinal cell ablation paradigms in zebrafish reveals shared and cell-specific regenerative responses

Kevin B. Emmerich[¶1,2], Steven L. Walker[¶3,4], Guohua Wang[¶1,5], David T. White[1], Fang Wang[1], Yong Teng[6], Zeeshaan Chunawala[1], Saumya Nimmagadda[1], Meera T. Saxena[1], Jiang Qian[1], and Jeff S. Mumm[1,2,3,7*]

1. Department of Ophthalmology, Wilmer Eye Institute, Johns Hopkins University, Baltimore, MD, USA
2. McKusick-Nathans Institute of the Department of Genetic Medicine, Johns Hopkins School of Medicine, Baltimore, MD, USA
3. Department of Cellular Biology and Anatomy, Medical College of Georgia, Augusta University, Augusta, Georgia, USA
4. Current address: School of Biomedical Sciences, The Chinese University of Hong Kong, N.T., Hong Kong
5. Current address: School of Computer Science and Technology, Harbin Institute of Technology, Harbin, China
6. Current address: Department of Hematology and Medical Oncology, Winship Cancer Institute, Emory University, Atlanta, GA, USA
7. Solomon H. Snyder Department of Neuroscience, Johns Hopkins University, MD, USA

¶Equal contribution, ordered alphabetically

*Corresponding author: jmumm3@jhmi.edu

Abstract

Zebrafish are a popular model for retinal regeneration studies due to the capacity of fish Müller glia (MG) to act as injury-induced retinal stem cells that replace lost neurons. In contrast, mammalian MG do not mount a regenerative response to cell loss. However, they do possess a dormant regenerative potential that can be activated. Increased understanding of how the regenerative potential of MG is regulated in zebrafish may aid efforts to promote retinal repair therapeutically. Developmental signaling pathways are known to coordinate regeneration following widespread retinal cell loss. Conversely, little is known about the regulation of "fate-biased" regeneration, a novel process following the loss of specific retinal cell types, i.e., paradigms more akin to retinal degenerative diseases. To address this knowledge gap, we compared transcriptomic responses between two selective cell ablation paradigms, targeted loss of either rod photoreceptors or retinal bipolar cells. Transcriptomic changes were assessed over twelve time points spanning early and late regeneration stages. 2,531 differentially expressed genes (DEGs) were identified. Early and late gene expression patterns were analyzed to identify paradigm-specific and shared genes and associated signaling pathways. Interestingly, the majority of DEGs were paradigm specific, suggesting fate-biased mechanisms attend each stage of the regenerative process, including stem cell activation. For example, early modulation of Notch signaling was implicated in the rod but not bipolar ablation paradigm. Among shared elements, the *socs* family genes, which provide negative feedback regulation of *jak/stat* signaling, were strongly upregulated. Additionally, a large number of DEGs related to immune-system function, with individual immune genes being largely paradigm specific. These data further support evidence of fate-biased regenerative processes following selective cell loss.

Author Summary

Blinding diseases are usually caused by the loss of specific types of neurons in the retina. In humans, once retinal neurons start to degenerate, they are unable to regenerate resulting in loss of sight. In zebrafish, however, retinal neurons are regenerated following damage resulting in restored vision. We have developed unique zebrafish models to study how individual retinal neuron types can be endogenously regenerated. Here, we compared gene expression changes occurring during the regeneration events of two different retinal cell types, rod photoreceptors and bipolar interneurons. Prior studies in zebrafish have examined gene expression changes following the death of multiple cells types at once, where regenerative processes appear to mimic retinal development. But much less is known about how specific cell types are replaced, a process recently termed fate-biased regeneration. Our direct comparison between two cell types showed us that most of the genetic events driving regeneration are unique to each cell type rather than shared between them. We identified a critical role for immune system related factors and pathways during this process with subtle differences arising between our two cell-specific paradigms. This information can help to inform future therapeutic attempts to replace disease-relevant retinal cell types in patients.

Introduction

Regenerative therapeutics aimed at replacing lost retinal cells have the potential to restore visual function. One category of therapeutics in development aims to stimulate endogenous retinal Müller glia (MG) to act as stem-like cells to replace lost neurons[1,2]. The capacity of MG to drive retinal repair differs markedly between species. In mammals, MG regenerative potential is intact but remains dormant unless exogenously stimulated. In contrast, zebrafish MG robustly regenerate lost retinal neurons[3]. Zebrafish are therefore an established model for exploring

mechanisms controlling MG regenerative potential, including factors that enhance the regenerative potential of mammalian MG[4–8]. Studies of the mechanisms regulating regeneration following widespread retinal cell loss have focused largely on developmental pathways and reprogramming factors[3,9–12]. In contrast, mechanisms governing responses to the loss of specific neuronal types are less well defined. Intriguingly, recent studies in zebrafish suggest that the loss of discrete retinal cell types elicits a fate-biased regenerative response; i.e., a more selective cell replacement program[13–16]. A deeper understanding of the mechanisms controlling fate-biased regeneration could facilitate novel regenerative therapeutic strategies.

Retinal regenerative research in fish has utilized three main injury paradigms: light-induced ablation[17–20], toxin-induced ablation[21,22] and mechanical wounding[23,24]. Early mechanical wounding studies involved surgical excisions of retinal quadrants which induce classic hallmarks of epimorphic regeneration: rapid wound closure and the formation of blastema-like zones of proliferative cells[23]. Other paradigms eliminate all or most cells in a retinal somal layer, e.g., light-induced ablation of rod and cone photoreceptor cells in the outer nuclear layer (ONL)[17–20], excitotoxin-induced ablation of interneurons in the inner nuclear layer (INL) and retinal ganglion cells (RGCs)[21,22]. Collectively, these studies have identified two injury-inducible stem cell niches in the teleost retina; ONL progenitor cells committed to producing rod cells[25,26], and an INL-localized retinal stem cell[27,28]. Subsequent studies demonstrated that the INL stem cells were Müller glia (MG), which function as injury-induced multipotent stem-like cells, capable of regenerating all retinal cell types[3,9–11]. Intriguingly, mammalian MG can also produce new neurons upon exogenous expression of neurogenic factors, such as *achaete-scute family bHLH transcription factor 1* (*ascl1*)[4,5] or inhibition of factors such as *nuclear factor I a/b/x* (*nfia/b/x*)

which sustain MG identity[29]. However, the types of neurons produced by mammalian MG are not typically well correlated to types of cells lost, being largely limited to bipolar cells upon *ascl1* overexpression for instance[30], though combinations of neurogenic factors are attempting to overcome this limitation[7]. These studies highlight the need to better understand how MG regenerative potential, and the fate choices of MG-derived neural progenitors, are regulated.

Retinal degenerative diseases typically involve the loss of discrete cell types. Thus, methods for replacing specific cell types are being sought as a strategy to restore vison to patients. To study how discrete cell types are regenerated we adapted a targeted cell ablation method, the nitroreductase (NTR) prodrug converting enzyme system[31–35], to zebrafish[36–41]. Transgenic expression of NTR renders cells susceptible to prodrugs, such as metronidazole (Mtz). Exposing fish to Mtz results in the selective loss of NTR-expressing cells by a DNA-damage induced cell death process[40–43]. This approach affords key advantages to the investigation of cellular regeneration. For instance, it can be genetically targeted to individual cell types and is prodrug inducible, allowing temporal synchronization of the regenerative process across many samples. While several mutant zebrafish lines exhibit cell-type specific losses, the lack of control over the onset and duration of cell death make it more difficult to profile regenerative responses in these models. Additionally, several retinal degeneration mutants also fail to regenerate[44] suggesting that a threshold of cell death is required to trigger retinal regeneration. Third, co-expression of a fluorescent reporter in NTR-targeted cells allows the regenerative process to be characterized in detail using *in vivo* time-lapse imaging[38,45] or quantified using high-throughput methods[39,46]. Using this approach, recent studies have shown that selective retinal cell loss elicits a fate-biased regenerative response[13–16]. This suggests selective and non-selective retinal cell regeneration

processes are differentially regulated. Using a selective rod cell ablation model akin to that deployed here, Hyde and colleagues have shown that the extent of cell loss is an additional factor impacting the responsiveness of retinal stem cell niches: limited rod cell loss leading to a response solely from ONL progenitors while widespread rod loss elicited responses in both ONL progenitors and MG cells[47].

Here, to increase understanding of fate-biased regenerative processes, we used time-resolved gene expression profiling to compare two retinal cell-type specific ablation paradigms in zebrafish. Comparisons between the targeted loss of either 1) bipolar cells[45], or 2) rod photoreceptors[46] involved profiling gene expression changes across 12 timepoints spanning the entire degenerative and regenerative process. Differential gene expression analysis across a total of 138 microarrays revealed both shared and paradigm-specific profiles. Paradigm-specific expression changes predominated at early and late time points, and shared expression profiles peaked at 24 and 32 hours after induction of cell loss. While paradigm-specific mechanisms were expected to be prevalent during late phases, corresponding to fate-biased progenitor cell differentiation, predominance at early time points suggests that MG stem cell activation involves signals unique to the cell type lost. In turn, this suggests the nature of degenerative events informs the regenerative process, consistent with lineage tracing experiments demonstrating fate-biased regeneration following selective cell loss[15]. Given the relevance to numerous degenerative diseases, greater understanding of the mechanisms regulating stem cell responses to selective cell loss and subsequent fate-biased regenerative processes is needed to inform the development of cell-type specific regenerative therapeutics.

Results

Specificity of NTR/Mtz-induced Cell Death and Assessments of Regeneration

To expand our understanding of mechanisms regulating the regeneration of discrete retinal cell types, gene expression changes attending two cell-specific ablation paradigms were compared. Specifically, transgenic zebrafish lines expressing NTR-reporter fusions in either a bipolar interneuron subtype (*nyctalopin* or *nyx*-expressing) or rod photoreceptor cells were used, referred to hereafter as "NTR-bipolar"[45] and "NTR-rod"[46], respectively (see Methods for full description). We first confirmed that NTR expression was specific to the targeted cell types within the retina. Prior studies have shown that expression in the NTR-bipolar line is restricted to retinal bipolar cells, with labeling of the pineal gland (epiphysis) in the brain as well[45,48]. For the NTR-rod line, immunohistochemistry confirmed that expression of the NTR-YFP fusion protein was restricted to rod cells, as previously shown for this line[40] and corresponding promoter element[49]. NTR-YFP expressing cells co-labeled with a rod-specific antibody marking outer segments, zpr-3[50,51] (Supp. Fig. 1a-a"), and were interdigitated with cells marked by a cone-specific antibody, zpr-1[52] (Supp. Fig. 1b-b"). Co-labeling levels with zpr-3 suggested that the majority of rod cells express the NTR-YFP transgene. The NTR-bipolar line uses the Gal4/UAS bipartite system to express two different transgenes, a membrane-tagged YFP and an NTR-mCherry fusion protein that enables cell ablation. In this background, NTR-mCherry expression is sporadic, with the number of NTR+ cells varying from low (~25 cells/retina) to high (hundreds of cells/retina)[45]. To account for this variability, mid-level expressing NTR-bipolar larvae (~100 targeted cells) were visually selected for these studies.

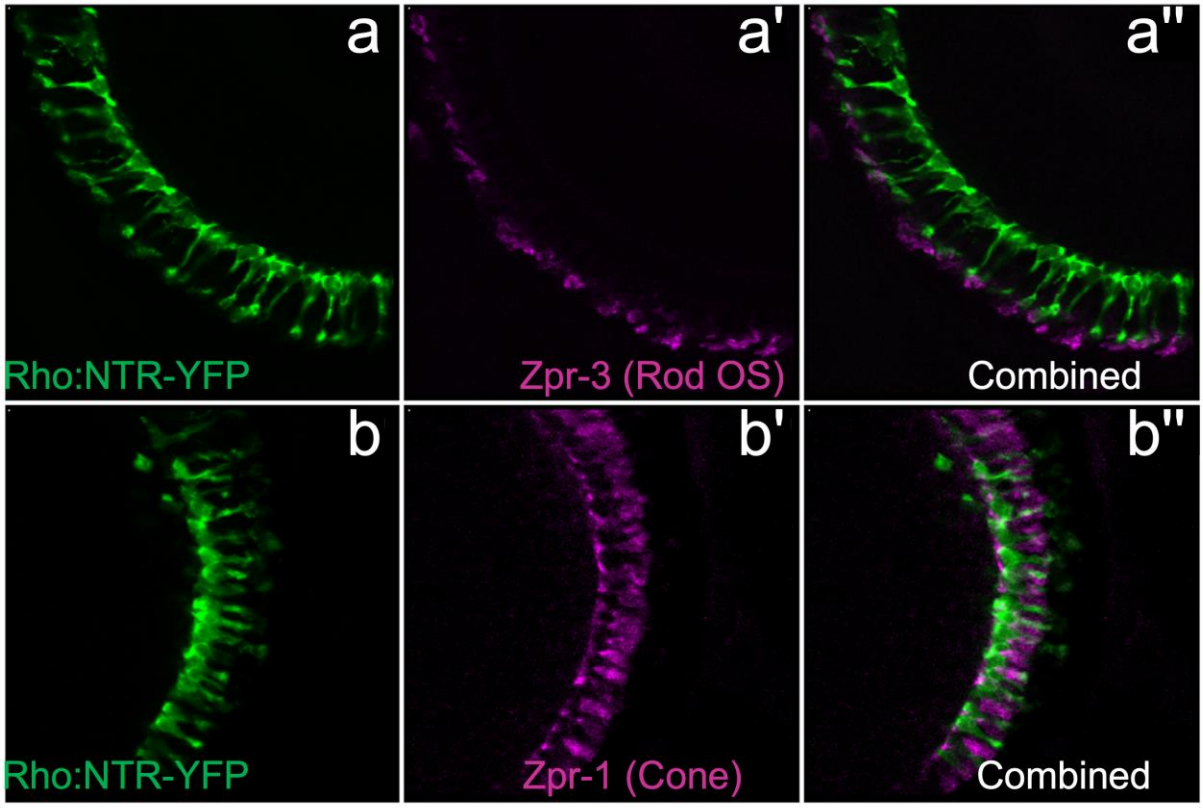

Supp. Fig. 1. Confirmation of NTR-rod transgene specificity

(a-a’’) Histological staining in the NTR-rod model showing transgenic Rho:YFP-NTR expression (green) along with antibody staining for rod outer segment marker Zpr-3 (purple). (b-b’’) Histological staining in the NTR-rod model showing transgenic Rho:YFP-NTR expression (green) along with antibody staining for cone marker Zpr-1 (purple).

We next verified that a 24 hr 10 mM Mtz prodrug treatment was sufficient to induce selective loss of NTR-expressing cells and that regeneration occurs upon Mtz washout. Confocal time series imaging was used to follow this process in individual NTR-bipolar and NTR-rod larva. (Fig. 1a-a’’ and b-b’’, respectively). After a 24 hr 10 mM Mtz treatment (from 6-7 days post-

fertilization, dpf) followed by 24 hr washout, NTR+ cells are largely absent or appear fragmented (Fig. 1a', b') in comparison to pre-treatment images (Fig. 1a, b). Four days after Mtz was removed (11 dpf), both NTR+ bipolar and rod cells had regenerated (Fig. 1a'', b''). DMSO controls showed sustained NTR expression in the absence of Mtz (Supp. Fig. 2a-a'', c-c''). Terminal deoxynucleotidyl transferase (TdT)-mediated dUTP nick end labeling (TUNEL)[53] staining confirmed layer-specific cell death in both paradigms (Fig. 1c-f series). Quantification showed a statistically significant increase in DNA damage (TUNEL staining) following Mtz exposures for both transgenic lines (Fig. 1g).

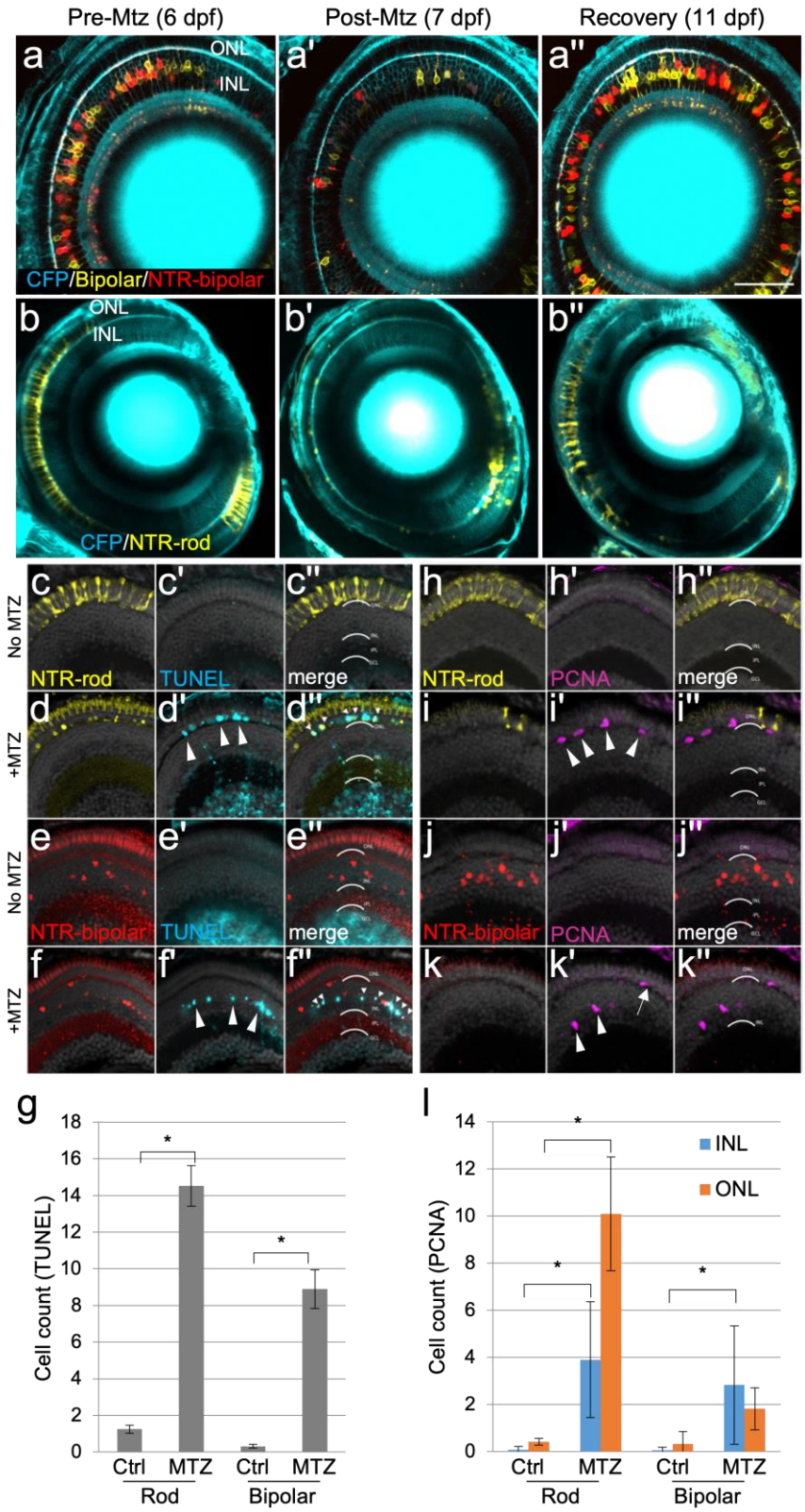
Pre-Mtz (6 dpf)
Post-Mtz (7 dpf)
Recovery (11 dpf)
a
a'
a''
ONL
INL
CFP/Bipolar/NTR-bipolar
b
b'
b''
ONL
INL
CFP/NTR-rod
No MTZ
+MTZ
No MTZ
+MTZ
c
c'
c''
NTR-rod
TUNEL
merge
h
h'
h''
NTR-rod
PCNA
merge
d
d'
d''
i
i'
i''
e
e'
e''
NTR-bipolar
TUNEL
merge
j
j'
j''
NTR-bipolar
PCNA
merge
f
f'
f''
k
k'
k''
g
Cell count (TUNEL)
Ctrl
MTZ
Ctrl
MTZ
Rod
Bipolar
l
Cell count (PCNA)
INL
ONL
Ctrl
MTZ
Ctrl
MTZ
Rod
Bipolar

191

Fig. 1. Two distinct NTR models enabling inducible cell specific ablation

(a-a'', b-b'') In vivo time-series imaging following the NTR-bipolar (a-a'') or NTR-rod (b-b'') response to metronidazole (Mtz) treatment to induce cell death and regeneration. Images were taken in the same fish at 6 dpf (before Mtz onset, a, b), 7 dpf (after treatment, a', b') and 11 dpf (following recovery, a'', b'').

(c-c'', d-d'', e-e''. f-f'') Representative histological staining for TUNEL (terminal deoxynucleotidyl transferase dUTP nick end labeling) at 7 dpf in uninjured NTR-rod larvae (c-c'') and Mtz treated NTR-rod larvae (d-d'') as well as in uninjured and Mtz-treated NTR-bipolar larvae (e-e'', f-f'', respectively).

(g) Quantification of TUNEL+ cell counts across the stained larval groups in both cell types.

(h-h'', i-i'', j-j''. k-k'') Representative histological staining for PCNA (proliferative cell nuclear antigen) at 9 dpf in uninjured NTR-rod larvae (h-h'') and Mtz treated NTR-rod larvae (i-i'') as well as in uninjured and Mtz-treated NTR-bipolar larvae (j-j'', k-k'', respectively).

(l) Quantification of PCNA+ cell counts across the stained larval groups in both cell types in either the inner or outer nuclear layer (INL, ONL).

Characterization of Retinal Stem Cell Niches Responding to Bipolar and Rod Cell Death

As the NTR-rod line consistently labels the majority of rod photoreceptor cells (Supp. Fig. 1), we anticipated rod cell loss would trigger proliferation in both the INL and ONL stem cell niches (multipotent MG and dedicated rod precursors, respectively), consistent with data from the Hyde lab using a similar transgenic line[47]. Conversely, we expected bipolar cell ablation would result in proliferation predominantly within the INL, i.e., localized to MG cells and daughter progenitor

cells. To test which retinal stem cell niche(s) were responsive to cell loss in the two ablation cell paradigms, Mtz-treated and DMSO control retinas were immunolabeled with proliferative cell nuclear antigen (PCNA) 72h post-onset of Mtz at 9 dpf (Fig. 1h-k series, during the peak of proliferation following ablation in our NTR models[38]. The data showed cell-specific trends, with a bias toward ONL, rod-committed precursor proliferation, after rod loss (Fig. 1i', arrowheads) and INL, MG/progenitor, proliferation following bipolar cell loss (Fig. 1k', arrowheads). On average more proliferation was seen in NTR-rod lines (~14 PCNA+ cells/retinal slice) versus NTR-bipolar fish (~5 PCNA+ cells/retinal slice, Fig. 1l). This difference was due to elevated levels of ONL proliferation following rod ablation as the amount of INL proliferation was similar in both paradigms (Fig. 1;). Proliferation within the INL in Mtz-treated NTR-rod lines was typically clustered near the periphery (Supp. Fig. 2h' where the density of cell loss was highest, consistent with increased rod cell death activating MG stem cells[47]. Note, many of the cells dividing in the ONL following bipolar cell ablation (Supp. Fig. 2g', arrowheads) were presumed to be MG-derived progenitors that had migrated to the ONL, not solely rod-committed ONL progenitors, consistent with prior studies[3].

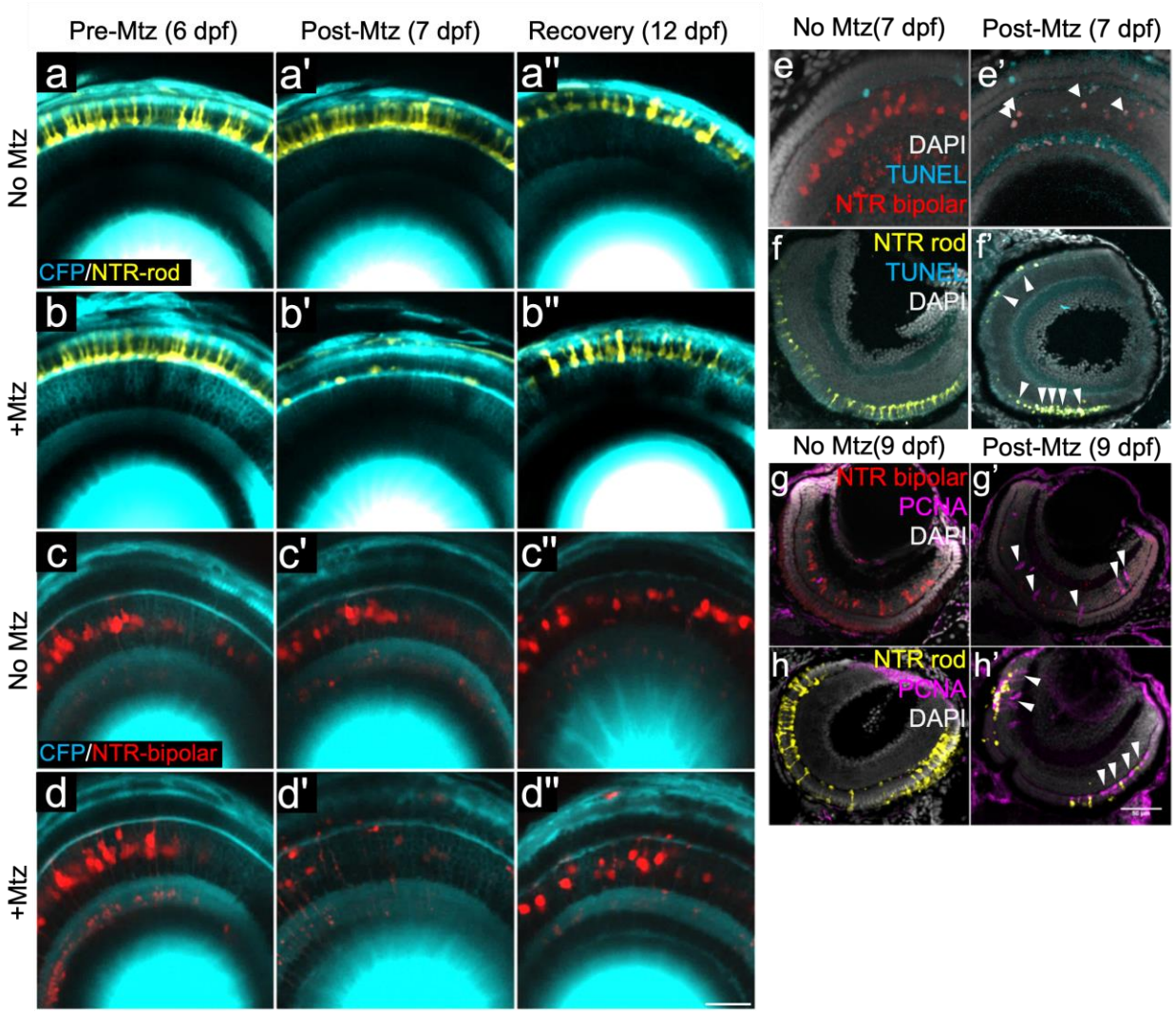

Supp. Fig. 2. Additional in vivo imaging and TUNEL/PCNA histological imaging

(a-a'', b-b'') In vivo time-series imaging following NTR-rod larvae that were uninjured (a-a'') or received Mtz (b-b''). Images were taken in the same fish at 6 dpf (before Mtz onset in +Mtz larvae), 7 dpf (after Mtz removal) and 11 dpf (following recovery).

(c-c'', d-d'') In vivo time-series imaging following NTR-bipolar larvae that were uninjured (c-c'') or received Mtz (d-d''). Images were taken in the same fish at 6 dpf (before Mtz onset in +Mtz larvae), 7 dpf (after Mtz removal) and 11 dpf (following recovery).

(e-e', f-f') Histological staining in uninjured and +Mtz eyes at 7 dpf for TUNEL in the NTR-bipolar (e-e') and NTR-rod (f-f') paradigms.

(g-g', h-h') Histological staining in uninjured and +Mtz eyes at 9 dpf for PCNA in the NTR-bipolar (g-g') and NTR-rod (h-h') paradigms.

Microarray Analysis of Two Cell-specific Regeneration Paradigms

We next turned to a differential gene expression comparison of our two retinal neuron ablation paradigms. To account for expression changes spanning cell loss and regeneration, eyes were collected from NTR-bipolar and NTR-rod larvae treated ±Mtz across a total of 12 time points, from 0 to 240 hours post ablation (hpa; Fig. 2a). As above, cell death was induced by the addition of 10 mM Mtz from 6 to 7 dpf (0 to 24 hpa), followed by wash out and recovery from days 7-16 dpf (24 to 240 hpa; Fig. 2a). To assess initial MG stem cell responses to retinal cell loss, early time points were emphasized by collecting samples every 8 hr from 0 to 48 hpa. Eight-hour intervals were used to minimize representation of gene expression changes due solely to circadian cycles. For the later time points, samples were collected at 60, 72, 96, 144, and 240 hpa. Across three biological repeats per time point, a total of 96 eyes were collected per time point for each paradigm (48 DMSO controls and 48 +Mtz samples, Supp. Table 1).

a

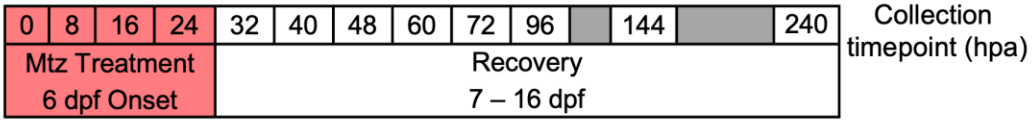

b

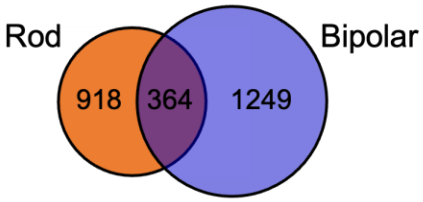

c

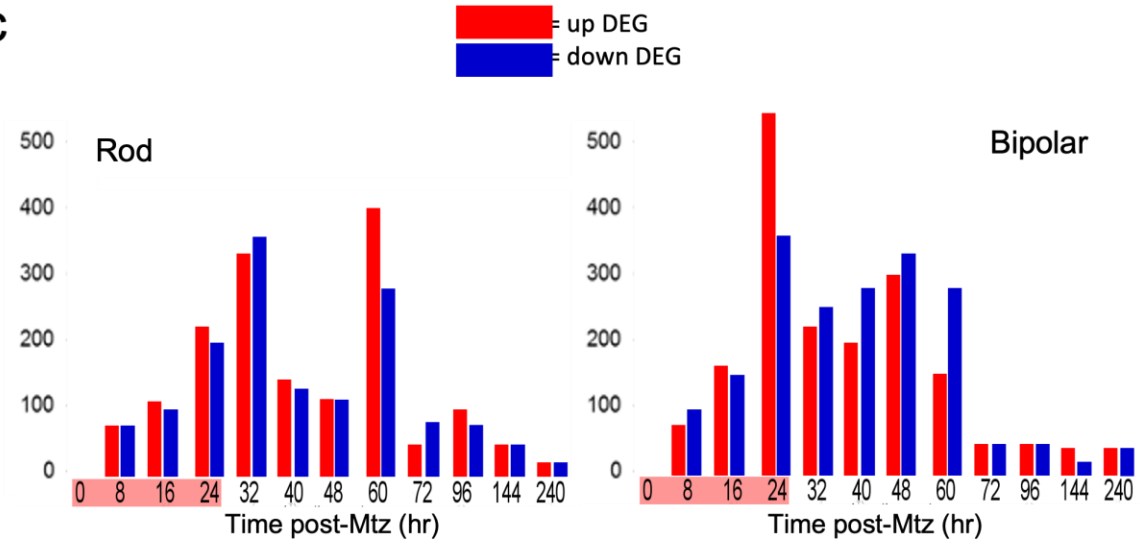

d

Top NTR-rod genes	fold (log2)	p-value	# of DEG timepoints
mala.2	2.49	1.70E-10	9
txn	1.87	6.25E-10	7
sepw2b	2.07	1.87E-09	8
prdx1	1.90	3.02E-09	7
wu:fb18f06	2.07	4.30E-09	8
gstp1	2.78	5.77E-09	7
cyp24a1	1.94	1.53E-08	3
stat2	1.68	1.57E-08	5
si:dkey-87o1.2	1.62	2.52E-08	5
nqo1	1.60	3.21E-08	5
cki	-2.66	6.65E-10	6
wu:fb15e04	-1.85	7.89E-10	7
nfil3-5	-1.44	1.86E-08	2
zgc:136930	-2.04	8.68E-08	6
cyt1l	-1.47	1.53E-07	6
ptprn2	-1.24	2.57E-07	2
cry1b	-1.78	2.68E-07	4
brdt	-1.46	4.57E-07	1
per3	-1.23	4.94E-07	4
myo3a	-1.34	6.71E-07	2

Top NTR-bipolar genes	fold (log2)	p-value	# of DEG timepoints
wu:fj05g07	3.05	3.66E-10	6
zgc:174888	2.14	4.46E-09	6
irf1b	2.23	6.42E-09	4
prdx1	1.89	7.59E-09	6
esm1	2.38	8.26E-09	6
atf3	2.45	2.21E-08	5
hsp70	1.77	3.23E-08	3
stat3	2.08	4.21E-08	5
irf9	1.75	5.81E-08	4
rpe65a	2.36	5.83E-08	1
si:ch211-195b15.7	-1.29	4.27E-07	8
Dr.12789.1.A1_at	-1.38	5.26E-07	8
pdca	-1.90	5.91E-07	6
arl3l2	-1.44	8.60E-07	7
pde6a	-1.76	9.99E-07	8
guca1b	-1.43	3.14E-06	6
s100w	-1.59	3.20E-06	3
gngt2a	-1.74	3.60E-06	3
zgc:162144	-1.66	4.62E-06	4
mb	-1.29	5.00E-06	2

256

Fig. 2. Microarray data collection, DEG identification and top hits

(a) Experimental design for tissue collection of whole eyes for microarray analysis. Treatment with Mtz for 24h was induced at 6 dpf following screening for NTR-rod+ or NTR-bipolar+ fish. Eyes were collected in triplicate at the following 12 timepoints including t0, t8, t16, 24, t32, t40, t48, t60, t72, t92, t144 and t240.

(b) Venn diagram illustrating the total number of differentially expressed genes (DEGs) unique to either cell type or shared between the two at all timepoints.

(c) Chart showing distribution of upregulated and downregulated DEGs in each paradigm.

(d) Top 10 up and downregulated genes across the entire data set based on p-value as well as the number of timepoints that gene was identified as differentially expressed out of 12.

Supp. Table 1. mRNA quality of samples collected for microarray analysis

Run	Cell Type	Concentration (ng)	mRNA Quality (RIN)
1	Rod	128.8 - 2327	6.6-10
2	Rod	109.2 - 992	7.8-9.8
3	Rod	136.0 - 1728	9.8-10
4	Bipolar	141.0 - 1029	5.9-9.4
5	Bipolar	145.4 - 990.8	8.2-9.3
6	Bipolar	204.5 - 685.4	8.4-9.4

Genetic Differences Observed Between Two Cell-specific Regeneration Paradigms

Using a 1.5-fold change and ≤ 0.05 *p*-value cutoff compared to expression values at 0 hpa, a total of 2,531 differentially expressed genes (DEGs) were observed across both paradigms. 918 and 1,249 DEGs were unique to the rod or bipolar cell ablation paradigm, respectively, and 364 DEGs were shared between the two (Fig. 2b). Plotting the number of DEGs per each time point showed two peaks at 32 and 60 hpa for the NTR-rod line, and a single peak at 24 hrs post ablation (hpa) for the NTR-bipolar line (Fig. 2c). Next, quantitative reverse transcriptase PCR (qRT-PCR) was used to validate gene expression changes for 8 genes per each paradigm at 0, 24, 48, 72 and 96 hpa (Supp. Fig. 3, primers used are listed in Supp. Table 2). The Janus kinase-signal transducer and activator of transcription (JAK/STAT) and Wnt pathway genes were selected for qRT-PCR analysis as both have been implicated in regeneration of the targeted cell types[10,54]. Temporally-resolved expression trends, rather than absolute fold change, were utilized for validation as differences in normalization methods have the potential to impact overall expression levels[55]. These data revealed only minor differences in expression patterns between the microarray and qRT-PCR suggesting the microarray data accurately reflect gene expression changes (Supp. Fig. 3). The top 10 up and down DEGs at all timepoints for each paradigm were then identified by lowest single *p*-value, many passing the DEG threshold at multiple timepoints

during our study (Fig. 2d).

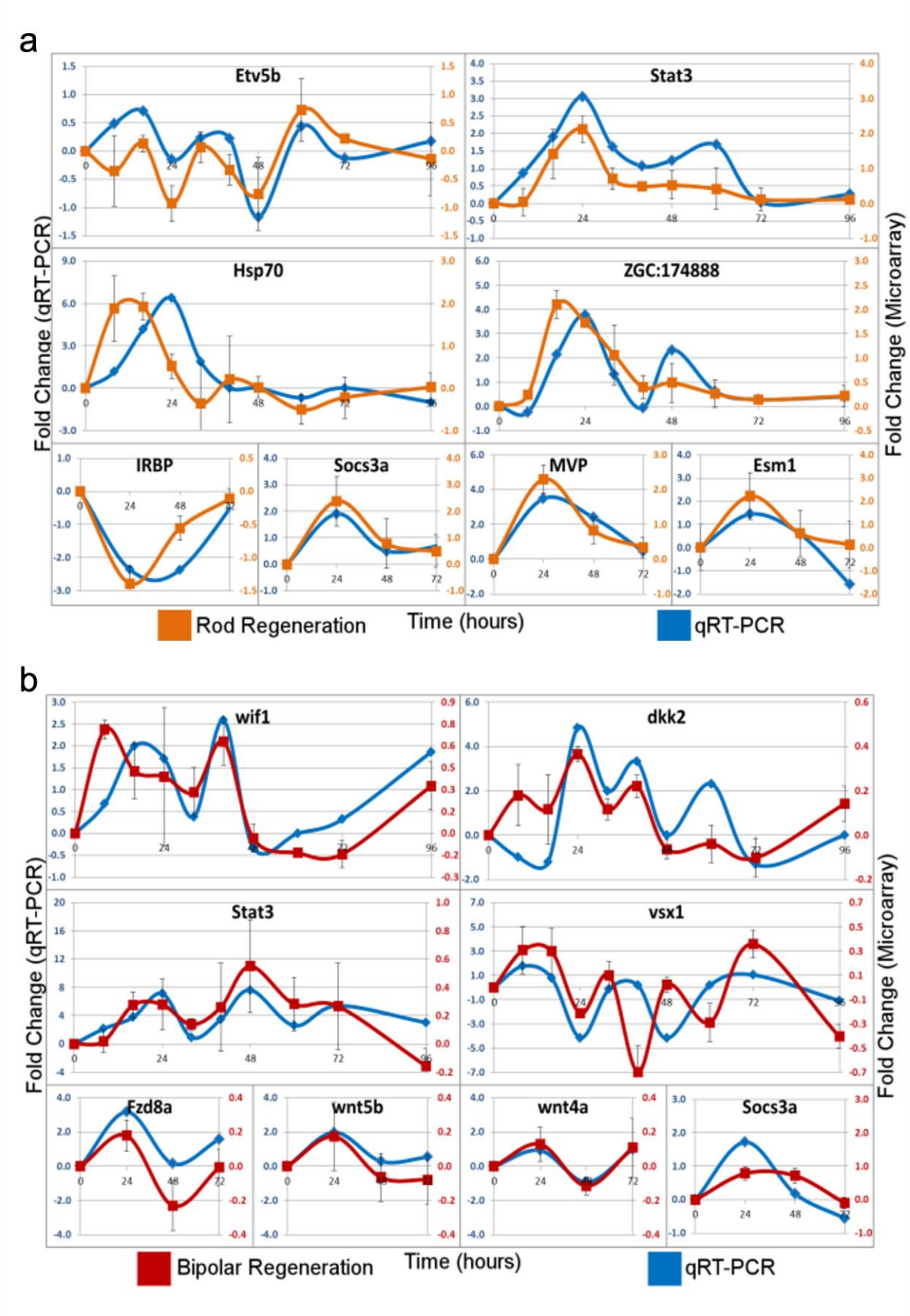
a
Etv5b
Stat3
Hsp70
ZGC:174888
IRBP
Socs3a
MVP
Esm1
Fold Change (qRT-PCR)
Fold Change (Microarray)
Rod Regeneration
Time (hours)
qRT-PCR
b
wif1
dkk2
Stat3
vsx1
Fzd8a
wnt5b
wnt4a
Socs3a
Fold Change (qRT-PCR)
Fold Change (Microarray)
Bipolar Regeneration
Time (hours)
qRT-PCR

290

Supp. Fig. 3. qRT-PCR validation of mRNA expression changes.

(a, b) A subset of tested genes were selected for validation using quantitative Reverse Transcription – Polymerase Chain Reaction (qRT-PCR). 8 genes were selected for a temporal analysis from 0-72h post Mtz in either the NTR-rod (A) or NTR-bipolar (B) paradigm with beta actin serving as a control.

Supp. Table 2. qPCR primers used

Gene	Ensembl ID	Sequence 5'-3'
stat3	ENSDARG00000022712	F, CTCATGCACAACGAAGCTGCTG
		R, TCCATGTCCGAGGTGAGGGATTCG
etv5b	ENSDARG00000044511	F, ACACCTGTCAATCACCCAGATGC
		R, AAAGCTGCCGATGGAACCTGTG
zgc:174888	ENSDARG00000077176	F, AGAAGCATGTCACCAACAGTGC
		R, TCGCACCCACTTCTTCCTTGAACAG
irbp	ENSDARG00000059163	F, GGAACAAAGTGGTGGACACTGACG
		R, GCATGCCCACCGATGTTATTTCTC
socs3a	ENSDARG00000025428	F, ACTCTGTGGGCACCAATCACTG
		R, CTGGTTTCTGTCGAACGTCTCC
hsp70	ENSDARG00000021924	F,GACCAGGGCAACAGAACAAC
		R, GGTCTCAATACCCAGAGACAGTGG
mvp	ENSDARG00000021242	F, GAGTGCAAAGAGTTACTGGTGAGG
		R, TCATGAGCTCCAGGCAGATACG

wif-1*	ENSDARG00000005541	F, GCCAGTGCGCTTTAAACCAACC
		R, TCACCTCAAATGCTGCCACACC
dkk2*	ENSDARG00000076420	F, ATGCCTCTTTTAAGCCGAAGTGC
		R,GCCTTTTTTGCGCTGTTTGG
fzd8a*	ENSDARG00000045444	F, TACTTCATGTGCCTTCTGGTGG
		R, TGGGCACTAAGACGTTAAGGC
wnt5b*	ENSDARG00000034894	F, CAGCTGACGGGCCTATCTCAGG
		R, AAAGCTCACCCTCACGGCACG
wnt4a*	ENSDARG00000071208	F, CAATGCGAGCAACTGGCTATAC
		R, AATGCAGCTTCCCTCGTACCTT
vsx1	ENSDARG00000056292	F, CCAGAGGACAGGATACAGGTATGG
		R, TTCTGGGAGTGGAATGGAGGT
β-actin**	ENSDARG00000037746	F, CGAGCAGGAGATGGGAACC
		R, CAACGGAAACGCTCATTGC

Transcriptomic Differences Following Regeneration of Uniquely Targeted Neurons

To identify differentially regulated signaling pathways at each time point, and across broader temporally-resolved expression patterns, several analysis methods were used. First, volcano plots and pathfindR[56] analyses were performed to reveal paradigm-specific and shared DEG-associated signaling pathways at each time point (Supp. Figs. 4-14). Volcano plots correlate log-fold changes in gene expression to *p*-values, with upregulated and downregulated DEGs indicated by orange and blue dots, respectively (Supp. Figs. 4a-14a). Venn diagrams show the

total number of DEGs unique to each paradigm and the number of shared DEGs (Supp. Figs. 4b-14b). Kyoto Encyclopedia of Genes and Genomes (KEGG) analysis via the pathfindR package revealed the top enriched pathways associated with either the rod or bipolar paradigm-specific DEGs, as well as shared DEGs (Supp. Figs. 4c-14c).

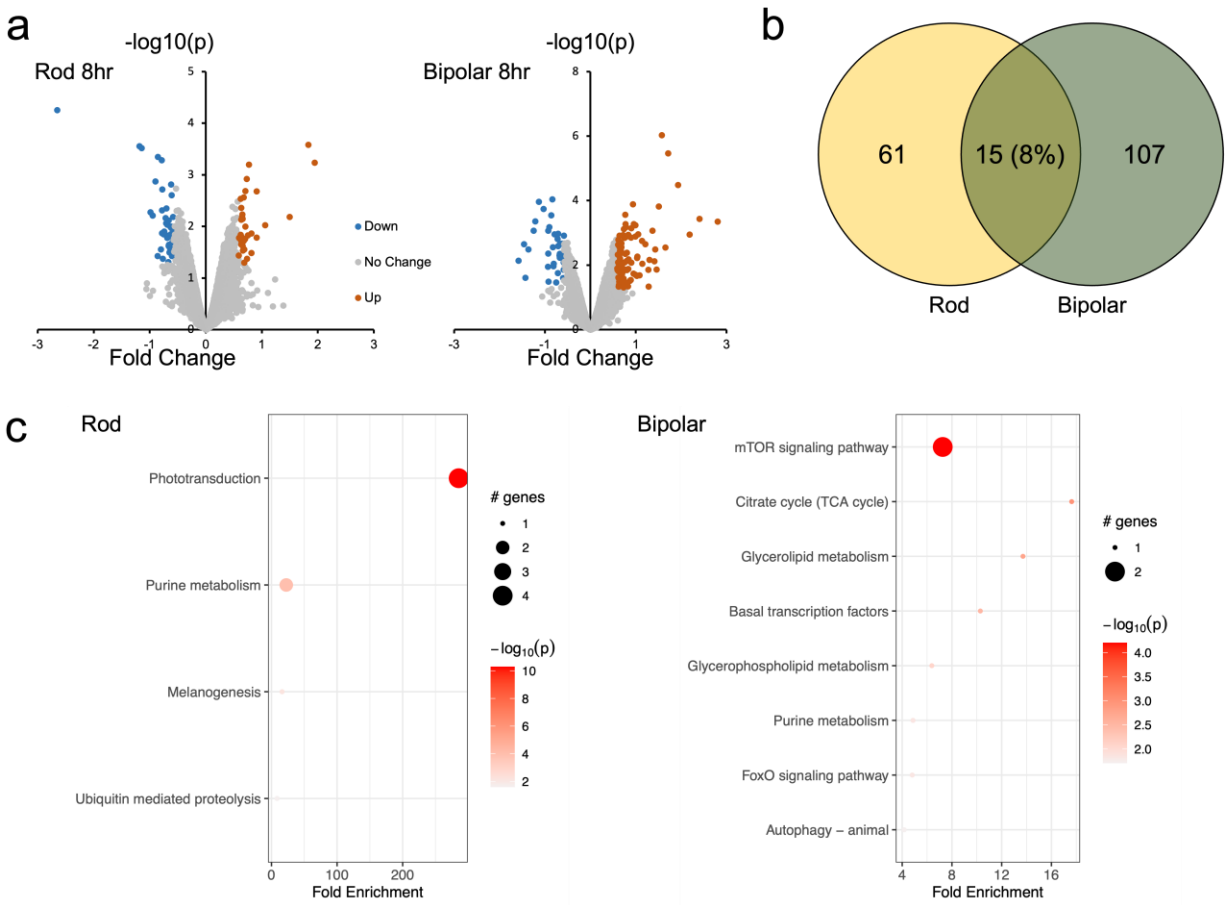

<u>Supp. Fig. 4. Analysis of DEGs and associated pathway terms at timepoint 8 hours following Mtz.</u>

(a) Volcano plot showing the identified up (orange) and down (blue) DEGs in both NTR-rod and NTR-bipolar treatment paradigms.

(b) Venn diagram showing the unique as well as shared (and % of shared) DEGs between the two paradigms.

(c) KEGG pathfindR identified significantly enriched pathways in the NTR-rod and NTR-bipolar paradigms.

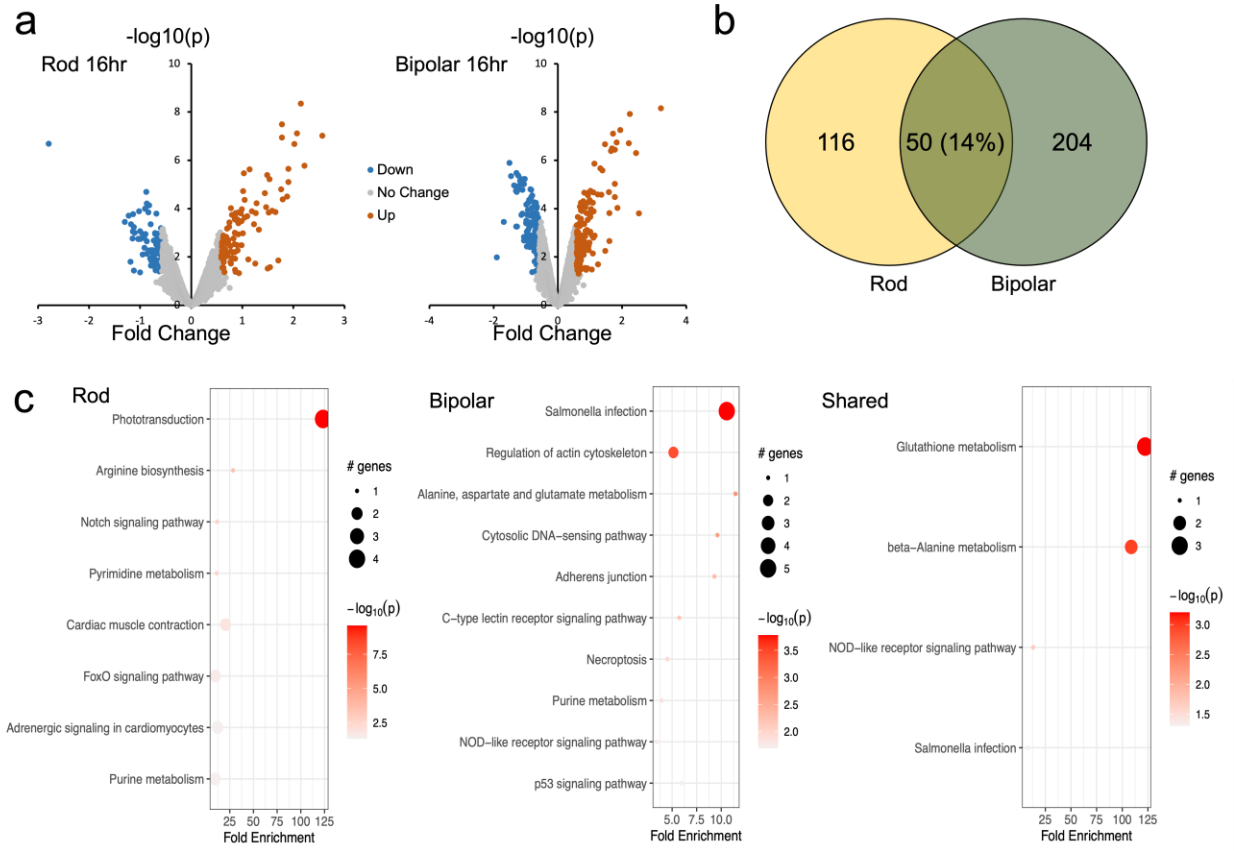

Supp. Fig. 5. Analysis of DEGs and associated pathway terms at timepoint 16 hours following Mtz.

(a) Volcano plot showing the identified up (orange) and down (blue) DEGs in both NTR-rod and NTR-bipolar treatment paradigms.

(b) Venn diagram showing the unique as well as shared (and % of shared) DEGs between the two paradigms.

(c) KEGG pathfindR identified significantly enriched pathways in the NTR-rod and NTR-bipolar paradigms as well as those shared between the two paradigms.

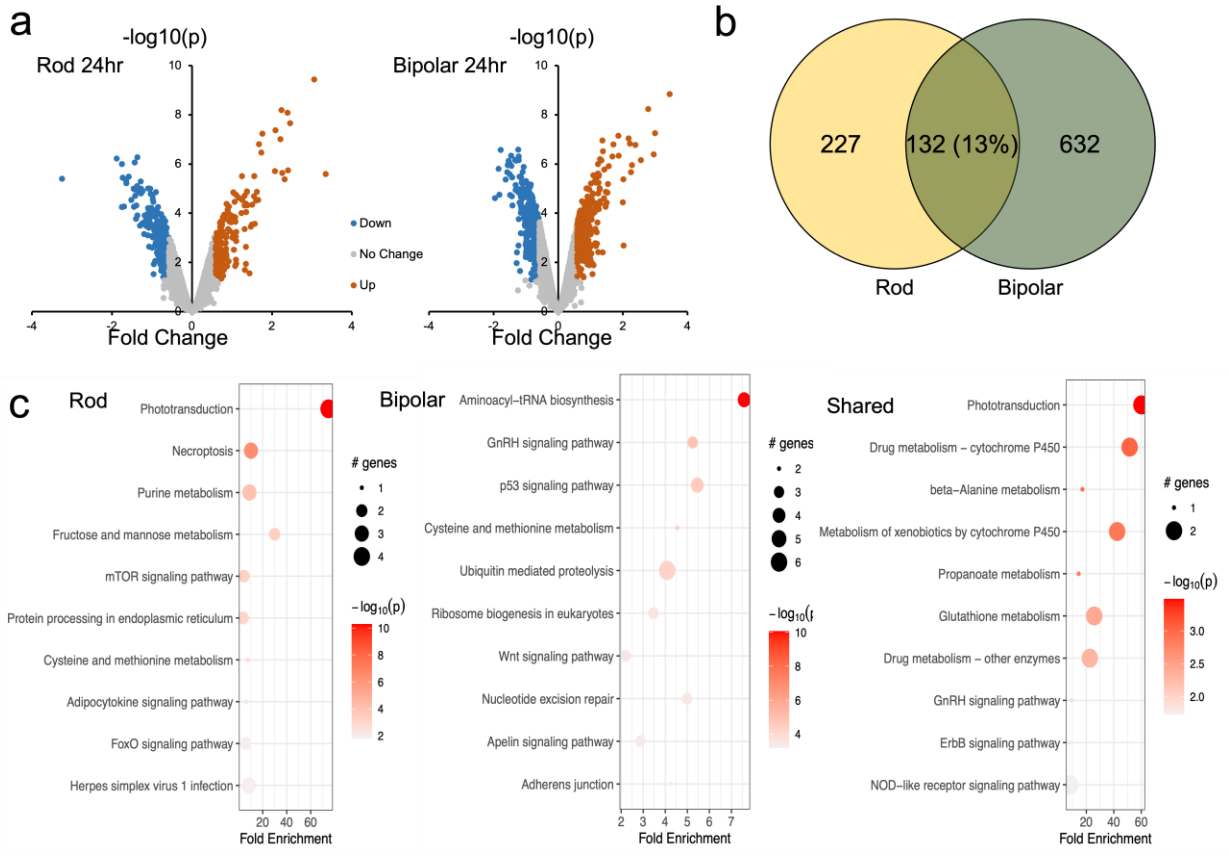

Supp. Fig. 6. Analysis of DEGs and associated pathway terms at timepoint 24 hours following Mtz.

(a) Volcano plot showing the identified up (orange) and down (blue) DEGs in both NTR-rod and NTR-bipolar treatment paradigms.

(b) Venn diagram showing the unique as well as shared (and % of shared) DEGs between the two paradigms.

(c) KEGG pathfindR identified significantly enriched pathways in the NTR-rod and NTR-bipolar paradigms as well as those shared between the two paradigms.

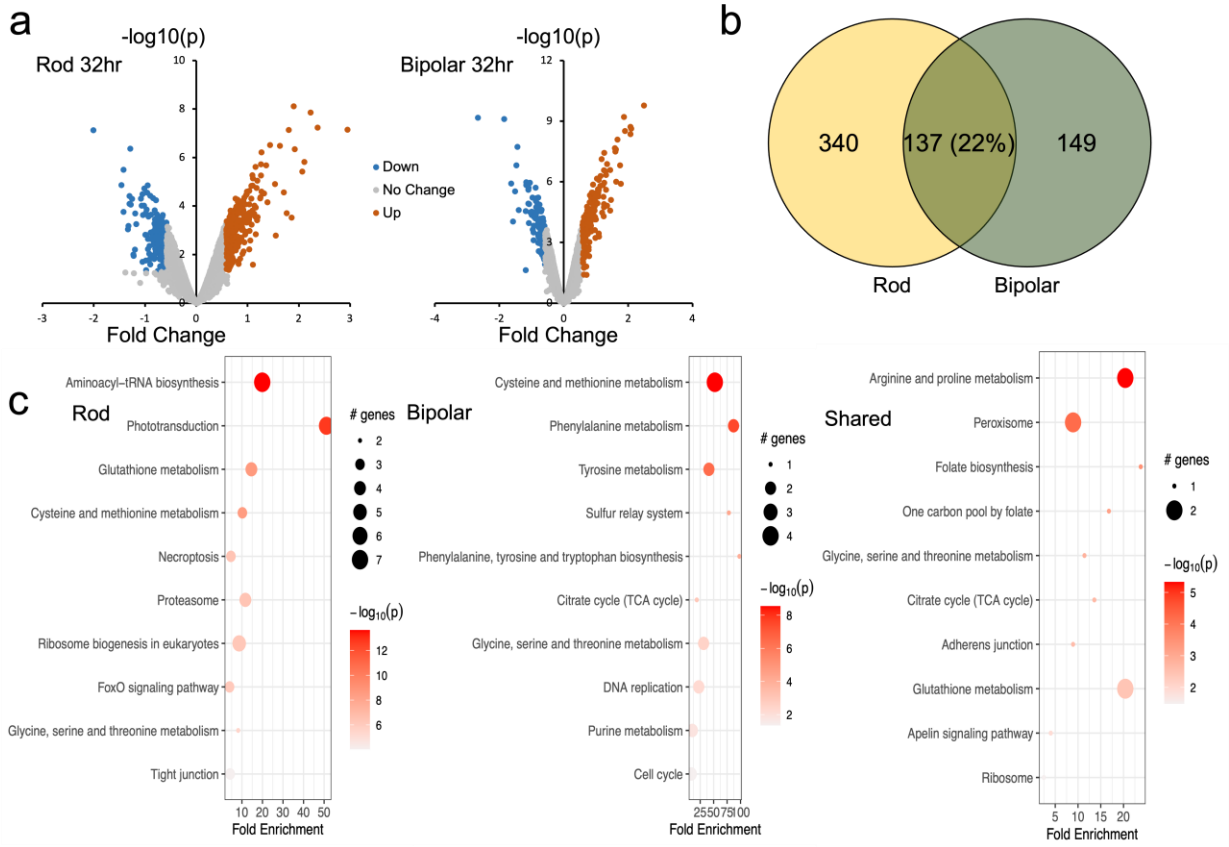

<u>Supp. Fig. 7. Analysis of DEGs and associated pathway terms at timepoint 32 hours following Mtz.</u>

(a) Volcano plot showing the identified up (orange) and down (blue) DEGs in both NTR-rod and NTR-bipolar treatment paradigms.

(b) Venn diagram showing the unique as well as shared (and % of shared) DEGs between the two paradigms.

(c) KEGG pathfindR identified significantly enriched pathways in the NTR-rod and NTR-bipolar paradigms.

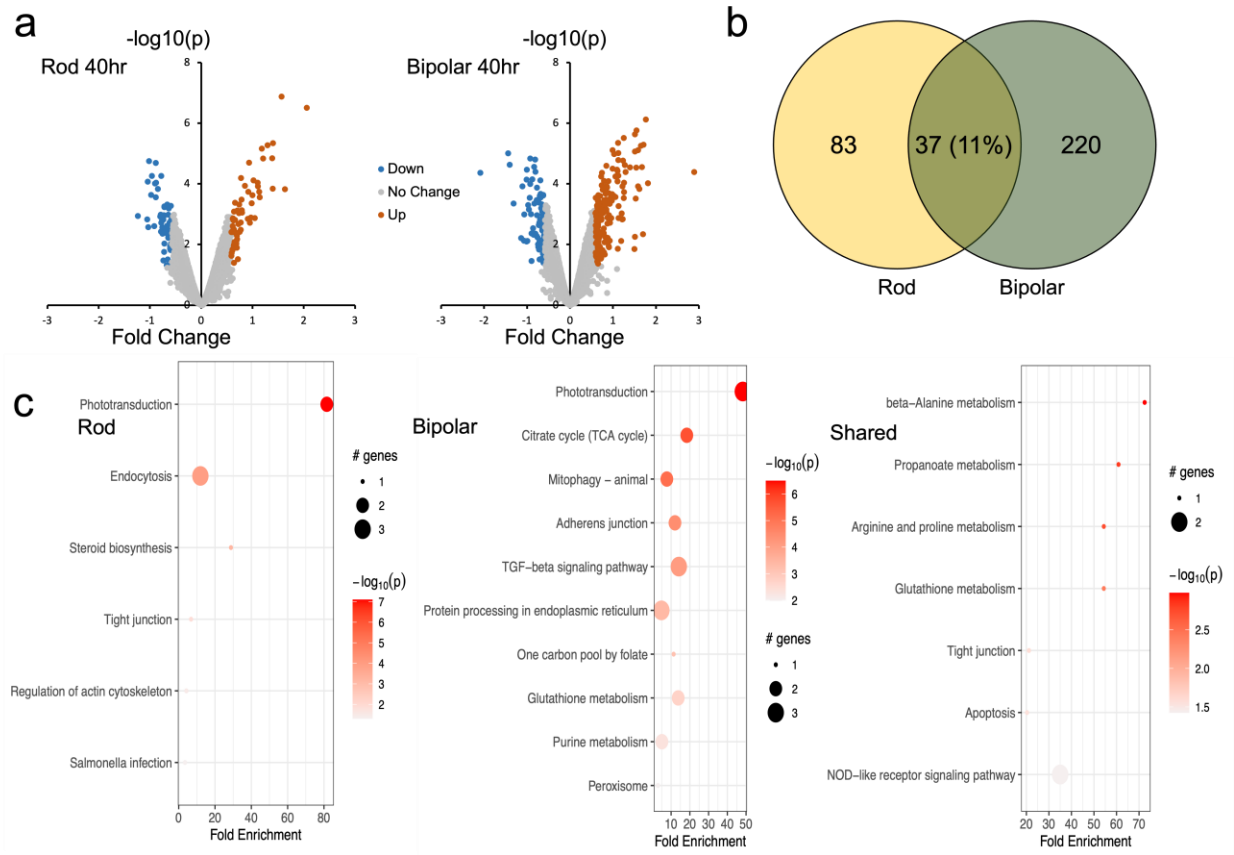

Supp. Fig. 8. Analysis of DEGs and associated pathway terms at timepoint 40 hours following Mtz.

(a) Volcano plot showing the identified up (orange) and down (blue) DEGs in both NTR-rod and NTR-bipolar treatment paradigms.

(b) Venn diagram showing the unique as well as shared (and % of shared) DEGs between the two paradigms.

(c) KEGG pathfindR identified significantly enriched pathways in the NTR-rod and NTR-bipolar paradigms as well as those shared between the two paradigms.

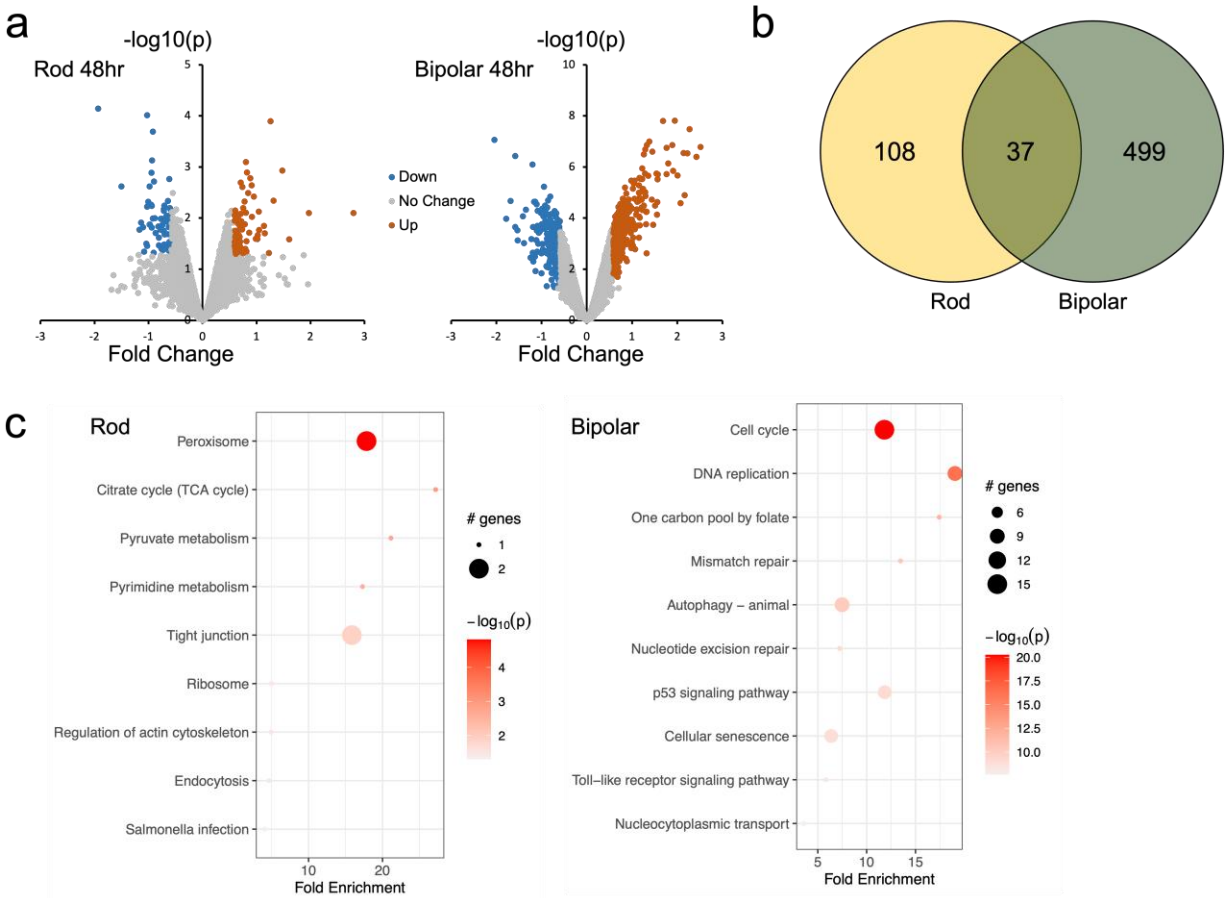

Supp. Fig. 9. Analysis of DEGs and associated pathway terms at timepoint 48 hours following Mtz.

(a) Volcano plot showing the identified up (orange) and down (blue) DEGs in both NTR-rod and NTR-bipolar treatment paradigms.

(b) Venn diagram showing the unique as well as shared (and % of shared) DEGs between the two paradigms.

(c) KEGG pathfindR identified significantly enriched pathways in the NTR-rod and NTR-bipolar paradigms.

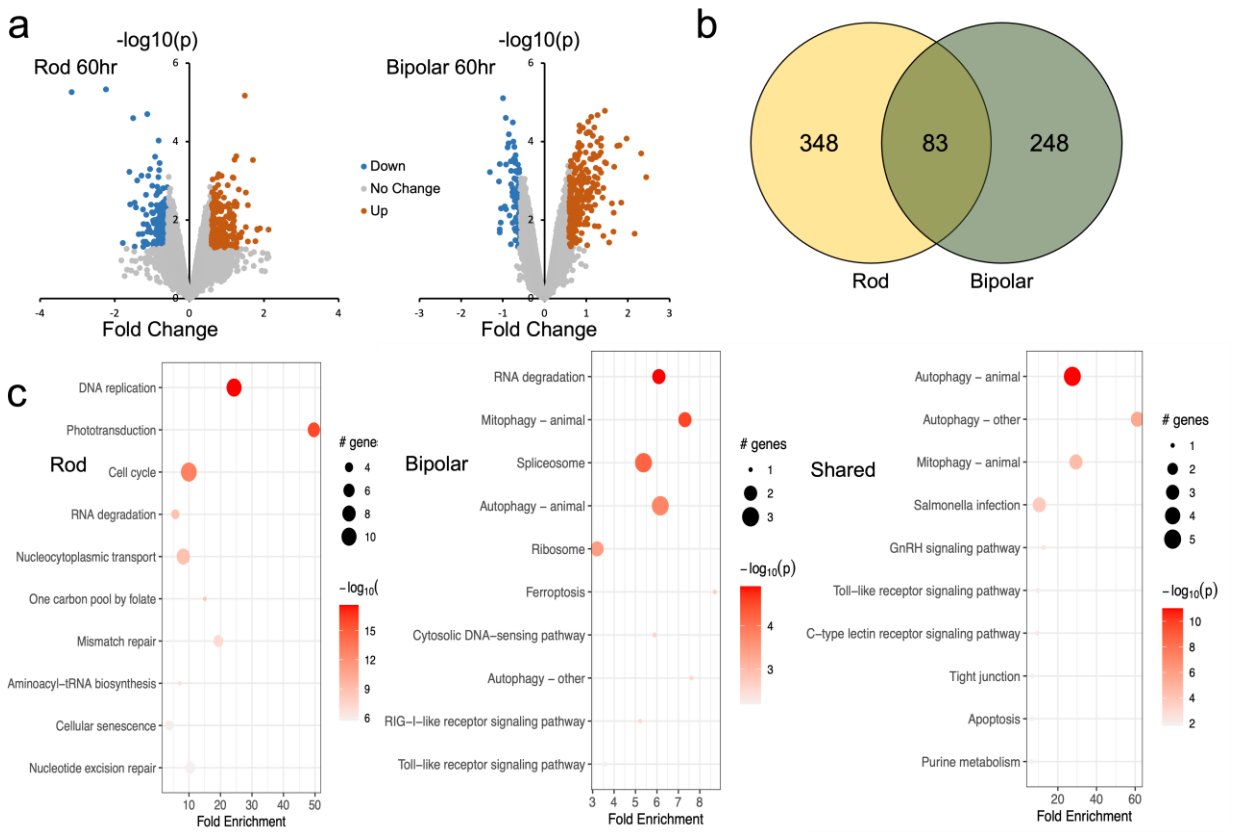

Supp. Fig. 10. Analysis of DEGs and associated pathway terms at timepoint 60 hours following Mtz.

(a) Volcano plot showing the identified up (orange) and down (blue) DEGs in both NTR-rod and NTR-bipolar treatment paradigms.

(b) Venn diagram showing the unique as well as shared (and % of shared) DEGs between the two paradigms.

(c) KEGG pathfindR identified significantly enriched pathways in the NTR-rod and NTR-bipolar paradigms as well as those shared between the two paradigms.

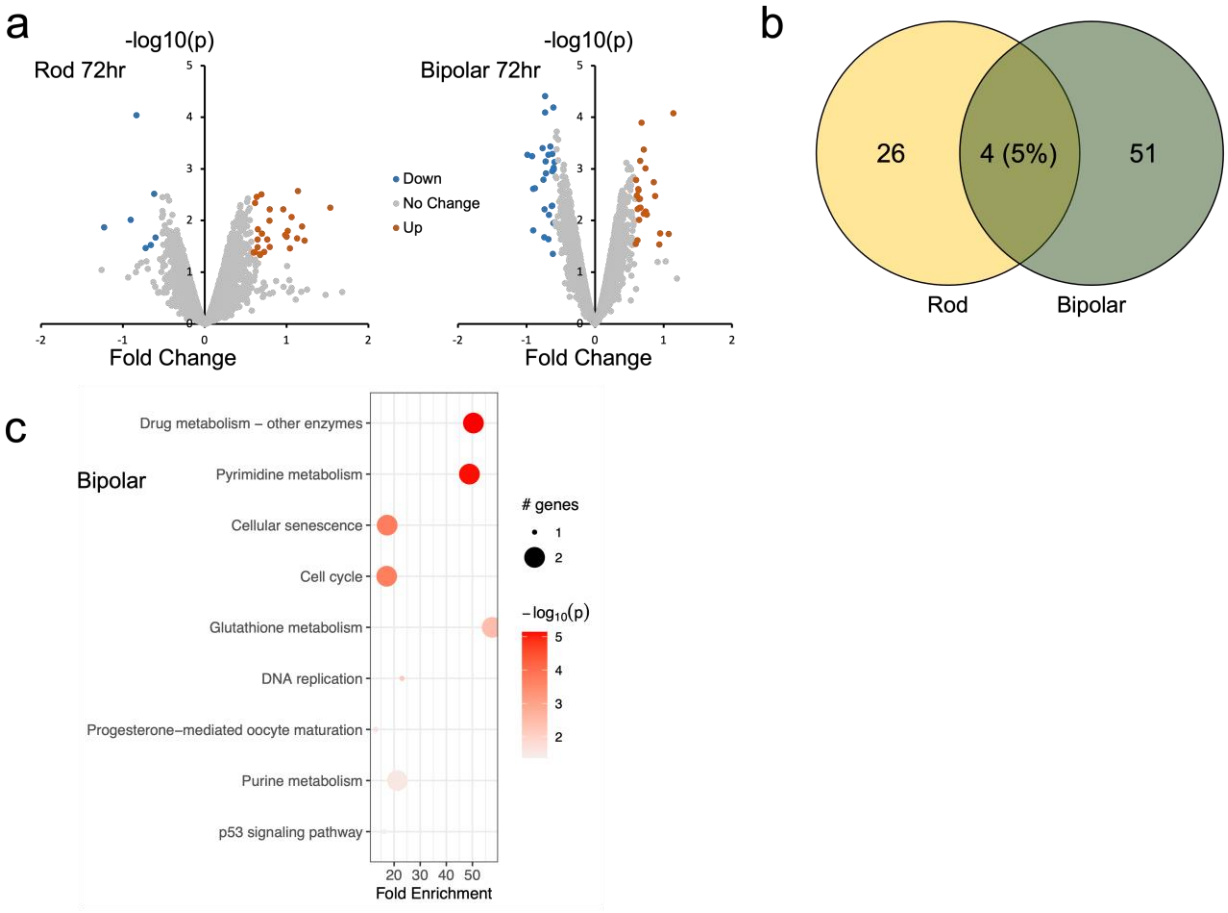

Supp. Fig. 11. Analysis of DEGs and associated pathway terms at timepoint 72 hours following Mtz.

(a) Volcano plot showing the identified up (orange) and down (blue) DEGs in both NTR-rod and NTR-bipolar treatment paradigms.

(b) Venn diagram showing the unique as well as shared (and % of shared) DEGs between the two paradigms.

(c) KEGG pathfindR identified significantly enriched pathways in the NTR-bipolar paradigm.

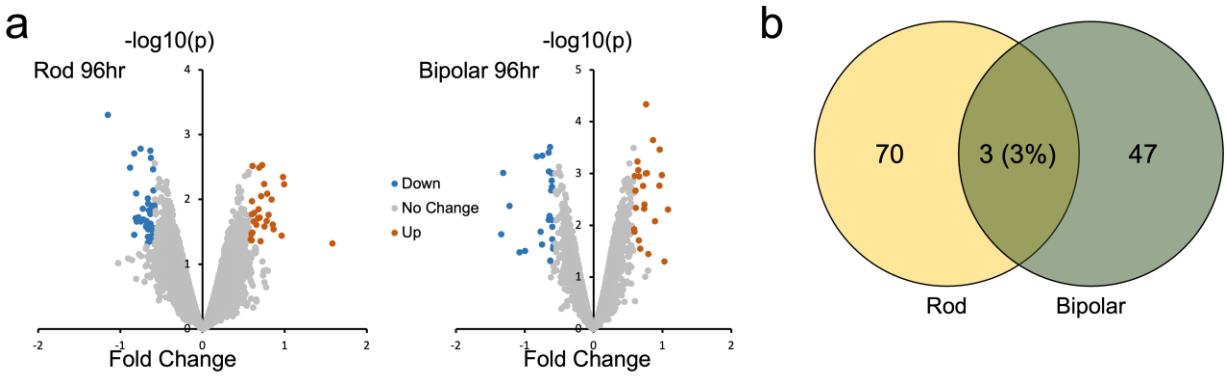

Supp. Fig. 12. Analysis of DEGs and associated pathway terms at timepoint 96 hours following Mtz.

(a) Volcano plot showing the identified up (orange) and down (blue) DEGs in both NTR-rod and NTR-bipolar treatment paradigms.

(b) Venn diagram showing the unique as well as shared (and % of shared) DEGs between the two paradigms.

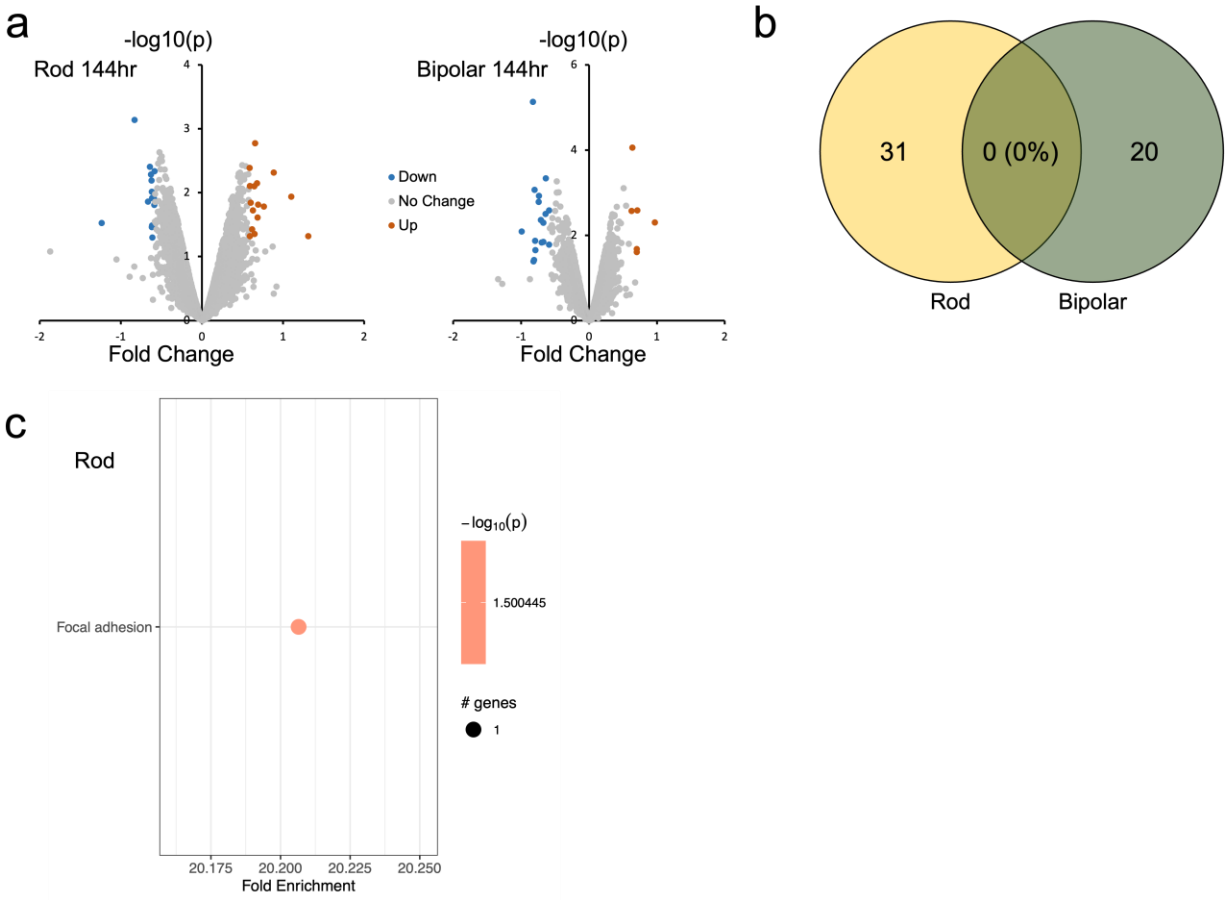

Supp. Fig. 13. Analysis of DEGs and associated pathway terms at timepoint 144 hours following Mtz.

(a) Volcano plot showing the identified up (orange) and down (blue) DEGs in both NTR-rod and NTR-bipolar treatment paradigms.

(b) Venn diagram showing the unique as well as shared (and % of shared) DEGs between the two paradigms.

(c) KEGG pathfindR identified significantly enriched pathways in the NTR-rod paradigm.

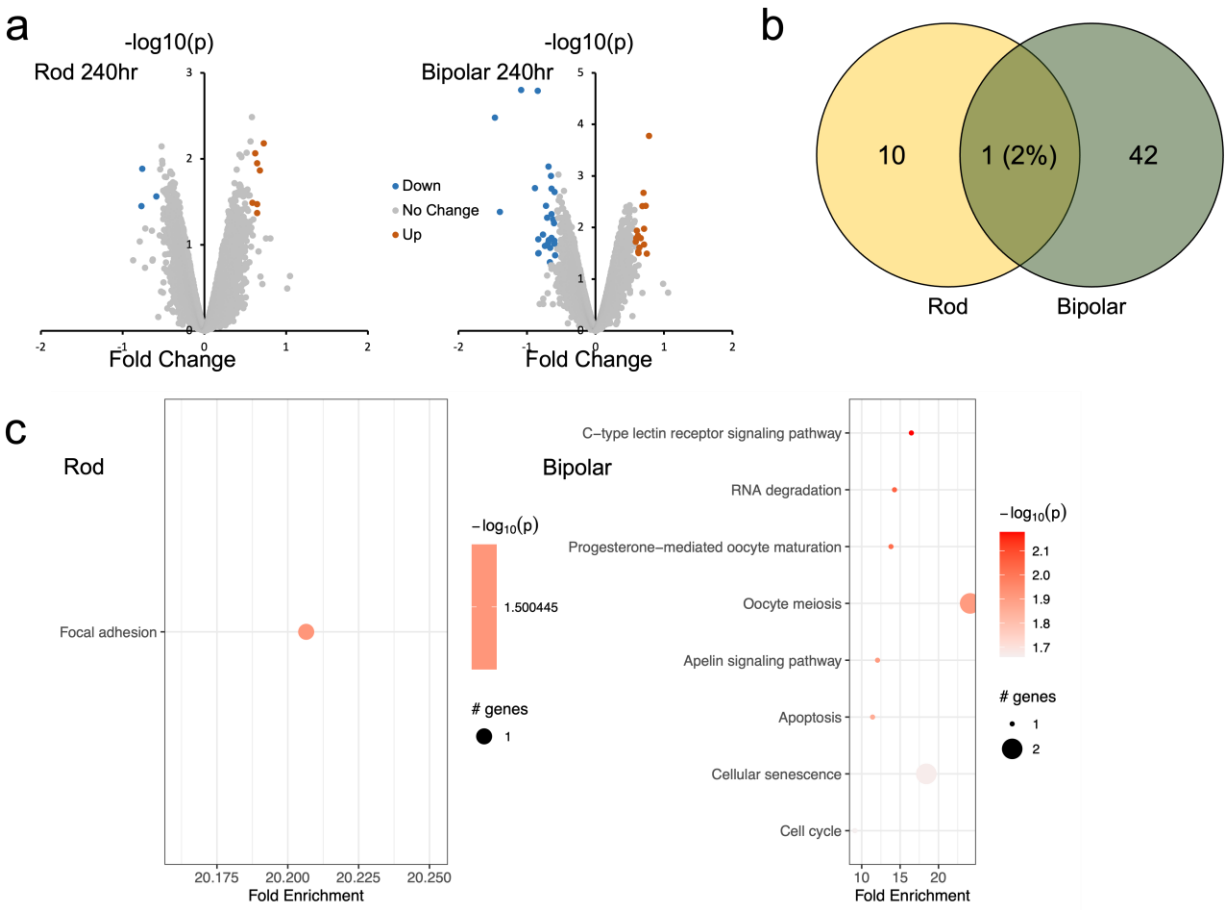

Supp. Fig. 14. Analysis of DEGs and associated pathway terms at timepoint 240 hours following Mtz.

(a) Volcano plot showing the identified up (orange) and down (blue) DEGs in both NTR-rod and NTR-bipolar treatment paradigms.

(b) Venn diagram showing the unique as well as shared (and % of shared) DEGs between the two paradigms.

(c) KEGG pathfindR identified significantly enriched pathways in the NTR-rod and NTR-bipolar paradigms.

We next looked at dynamically coordinated changes in gene expression, identifying DEGs whose expression profile fit one of four gaussian-type patterns during the regenerative process: increased (up early) or decreased (down early) from16 to 32 hpa, and increased (up late) or decreased (down late) from 48 to 72 hpa (Fig. 3a). Notably, this captured the majority of DEGs observed. Heatmaps are shown for the top 50 DEGs for each pattern in both the NTR-rod and NTR-bipolar paradigms (Fig. 3b,c). The two reciprocally regulated DEG patterns – up/down early (Fig. 4) and up/down late (Fig. 5) – were evaluated using KEGG, Gene Ontology (GO) and Ingenuity Pathway Analysis (IPA). For early pattern DEGS (Fig. 4a), the top 10 pathfindR KEGG terms were plotted for rod-specific, bipolar-specific and shared gene sets (Fig. 4b-d). Predictably for the rod paradigm, phototransduction was the most enriched term. Additional rod-specific KEGG pathways included RNA degradation, proteosome, and necroptosis (Fig. 4b). For the bipolar paradigm, p53 signaling was the most enriched term, other pathways included autophagy, nucleoside excision repair, and cysteine and methionine metabolism (Fig. 4c). Shared KEGG pathway terms for early pattern DEGs included phototransduction, mTor signaling, and glutathione metabolism (Fig. 4d). Gene Ontology (GO) analysis of the same datasets revealed additional terms, such as circadian rhythm and ncRNA processing for the rod paradigm, cellular apoptotic processes and response to stress for the bipolar paradigm, and response to temperature stimulus and DNA conformation change among shared terms (Fig. 4e-g). Lastly, IPA was used to generate unsupervised networks from the early DEG lists for the NTR-rod and NTR-bipolar paradigms (Fig. 4h,i). For the rod paradigm, signal transducer and activator of transcription 3 (STAT3) was identified as the central mediator of the early DEG network along with multiple cytokine terms (e.g, interleukin-1b and 6, IL-1B, IL-6) and associated terms for the oxidative stress response (Fig. 4h). In the bipolar paradigm, the central mediator was peroxisome

proliferator-activated receptor gamma (PPARG), other noteworthy genes included tumor protein 53 (TP53), the cytokine IL-10, and STAT5a/b (Fig. 4i). We then produced a summary bar chart of all related immune terms identified from IPA. Early pattern IPA-implicated pathways of the rod paradigm included JAK family kinases, chemokine (C-X-C motif) receptor 4 (CXCR4), IL-6, interferon, and iNOS signaling, as well as multiple other IL-family cytokines (Supp. Fig. 15a). For the bipolar paradigm, early pattern IPA terms included similar IL-family cytokines but also added prolactin and leukocyte extravasation signaling, as well as phagosome maturation (Supp. Fig. 15b). Combined, KEGG, GO, and IPA analysis revealed that factors implicated in regulating the early stages of regeneration are linked more to the loss of individual retinal cell types than to a common signature across cell types.

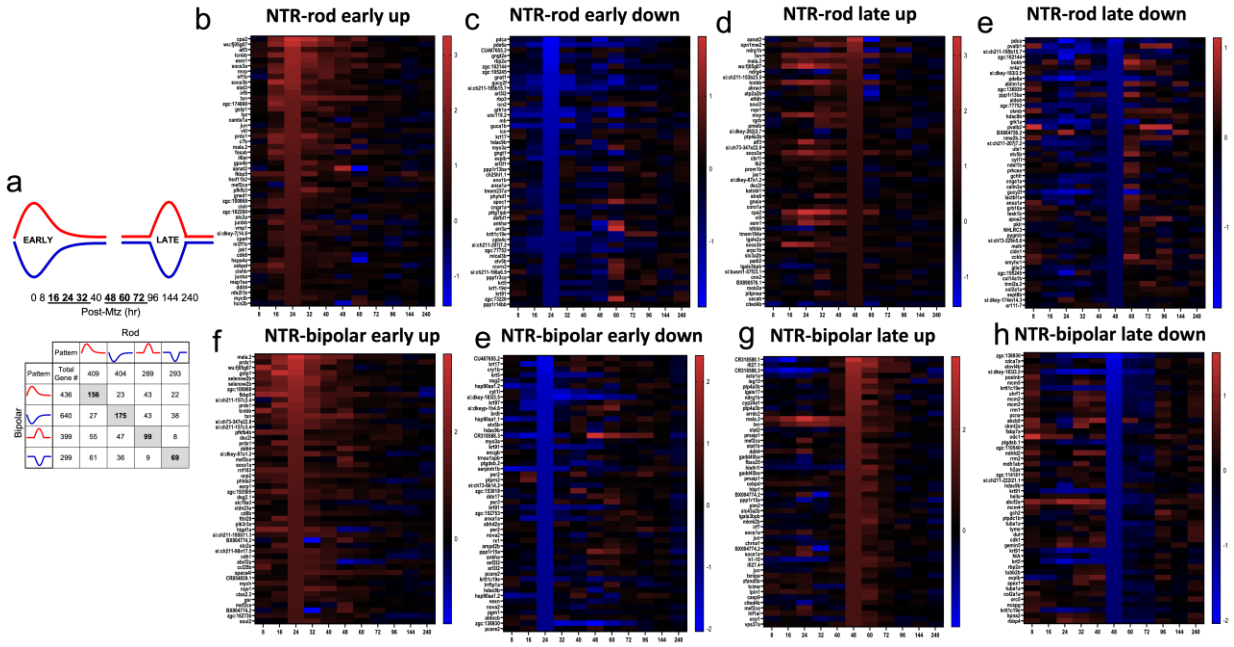

Fig. 3. Identification of early and late DEG patterns and heatmaps for top DEGs in each.

(a) DEGs for each paradigm were split into upregulated (red) and downregulated (blue) as well as early (16-32h) and late (48-72h) based on peaks in figure 2. The distribution of DEGs in these 8 patterns is shown in terms of unique and shared DEGs across both cell types.

(b-h) The top 50 genes are plotted in heatmaps as a function of the largest fold changes at the middle timepoint in each pattern (24h and 60h) to demonstrate top genes defining each 8 patterns (NTR-rod and NTR-bipolar for patterns early-up, early-down, late-up and late-down).

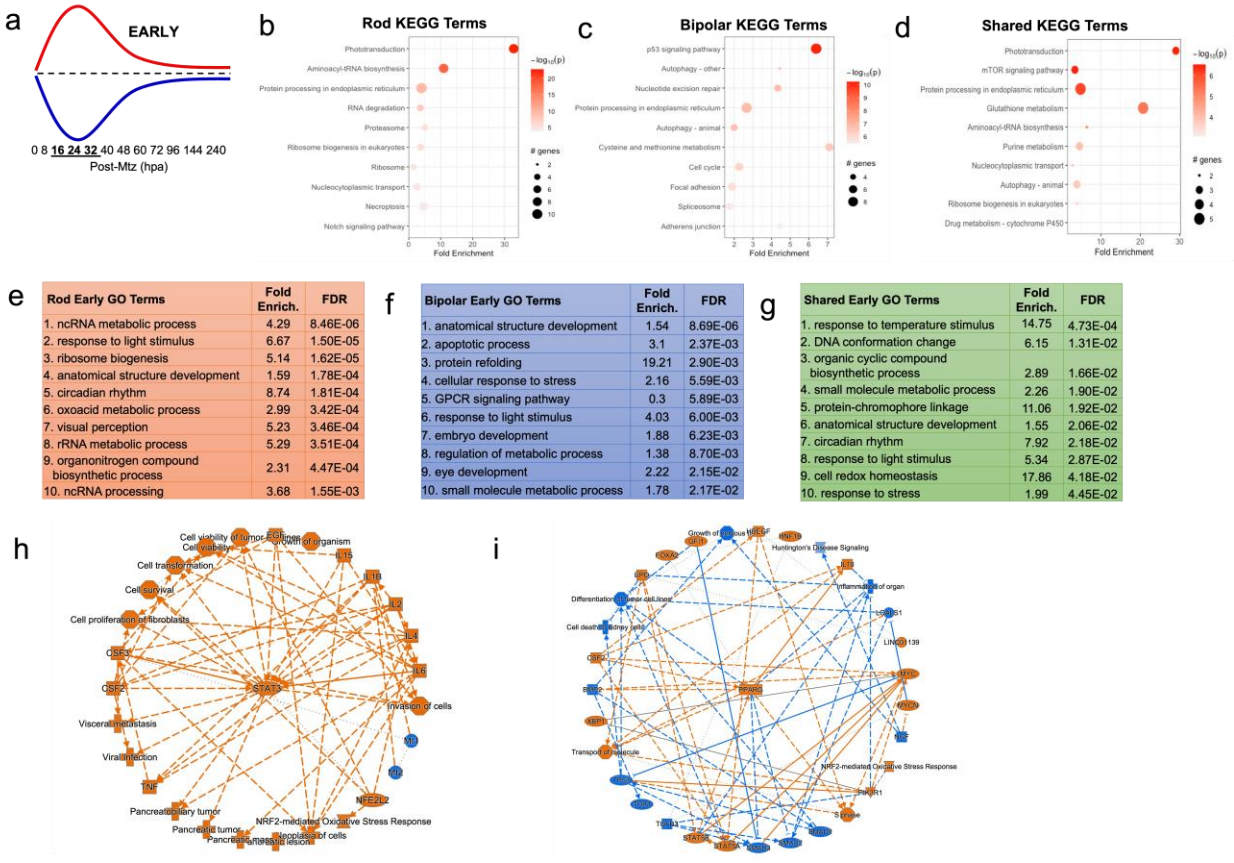

Rod Early GO Terms	Fold Enrich.	FDR
1. ncRNA metabolic process	4.29	8.46E-06
2. response to light stimulus	6.67	1.50E-05
3. ribosome biogenesis	5.14	1.62E-05
4. anatomical structure development	1.59	1.78E-04
5. circadian rhythm	8.74	1.81E-04
6. oxoacid metabolic process	2.99	3.42E-04
7. visual perception	5.23	3.46E-04
8. rRNA metabolic process	5.29	3.51E-04
9. organonitrogen compound biosynthetic process	2.31	4.47E-04
10. ncRNA processing	3.68	1.55E-03

Bipolar Early GO Terms	Fold Enrich.	FDR
1. anatomical structure development	1.54	8.69E-06
2. apoptotic process	3.1	2.37E-03
3. protein refolding	19.21	2.90E-03
4. cellular response to stress	2.16	5.59E-03
5. GPCR signaling pathway	0.3	5.89E-03
6. response to light stimulus	4.03	6.00E-03
7. embryo development	1.88	6.23E-03
8. regulation of metabolic process	1.38	8.70E-03
9. eye development	2.22	2.15E-02
10. small molecule metabolic process	1.78	2.17E-02

Shared Early GO Terms	Fold Enrich.	FDR
1. response to temperature stimulus	14.75	4.73E-04
2. DNA conformation change	6.15	1.31E-02
3. organic cyclic compound biosynthetic process	2.89	1.66E-02
4. small molecule metabolic process	2.26	1.90E-02
5. protein-chromophore linkage	11.06	1.92E-02
6. anatomical structure development	1.55	2.06E-02
7. circadian rhythm	7.92	2.18E-02
8. response to light stimulus	5.34	2.87E-02
9. cell redox homeostasis	17.86	4.18E-02
10. response to stress	1.99	4.45E-02

Fig. 4. Pathway analysis of early DEG pattern in both paradigms.

(a) Curve demonstrating expression pattern for early upregulated (red) and downregulated (blue) genes along our timepoints.

(b-d) Top 10 enriched KEGG pathway terms including p-value and # of genes found as DEGs in the NTR-rod (b), NTR-bipolar (c) or from shared DEGs across both paradigms (d).

(e-g) Top 10 enriched Gene Ontology pathway terms including fold enrichment and false discovery rate in the NTR-rod (e), NTR-bipolar (f) or from shared DEGs across both paradigms (g).

(h-i) Unsupervised gene networks produced from ingenuity pathway analysis for DEGs in the NTR-rod (h) and NTR-bipolar (i) paradigm. Orange indicates upregulated gene/pathway term while blue indicates downregulated.

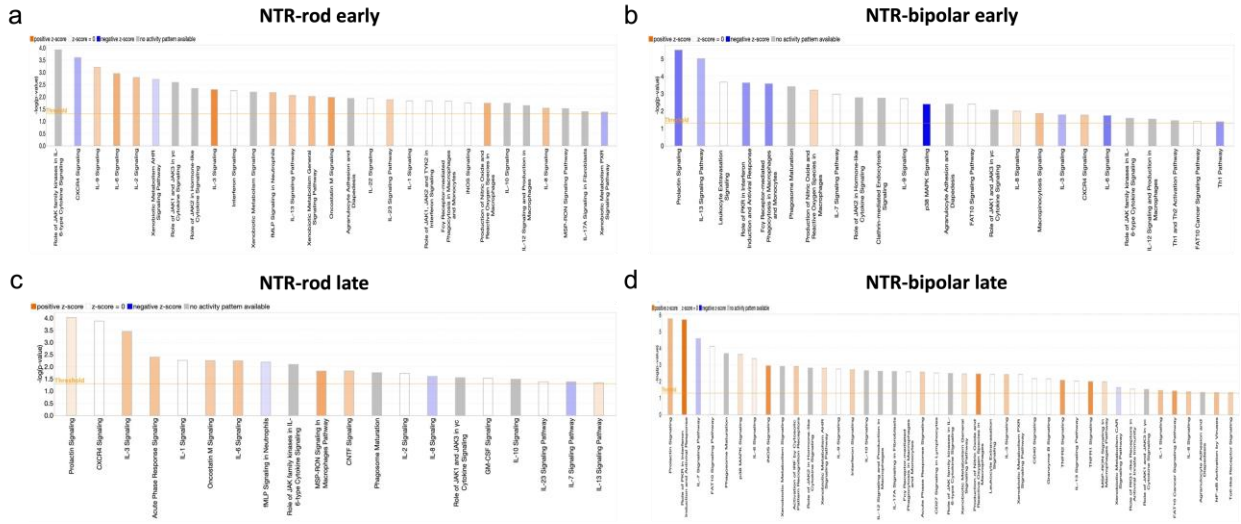

Supp. Fig. 15. Immune related terms identified from IPA for each pattern.

(a-d) IPA was used to test for enriched immune related pathway terms from DEGs for each pattern including NTR-rod early (a), NTR-bipolar early (b), NTR-rod late (c) and NTR-bipolar late (d).

The same analysis methods were used to evaluate late pattern DEGs (Fig. 5a). A subset of top KEGG terms stayed consistent with early pattern DEGs including phototransduction and RNA degradation for the rod paradigm, autophagy and p53 for the bipolar paradigm, and also autophagy for shared genes (Fig, 5b-d). The top enriched KEGG terms were DNA replication and cell cycle for the rod and bipolar paradigms, respectively. While new terms included mismatch repair for rods, Toll-like receptor signaling for bipolars, and cellular senescence for the shared set (Fig. 5b-d). Enriched GO terms similarly included some overlap with early pattern terms (Fig. 5e-g), new rod GO terms included ribosome biogenesis, nuclear RNA surveillance,

and sno(s) RNA processing (Fig. 5e). New bipolar terms included oxoacid metabolic process, circadian rhythm, and response to peptide hormone (Fig. 5f). Fewer shared DEGs in the late pattern data lead to fewer enriched GO terms, however, the majority were new including cellular response to DNA damage and regeneration (Fig. 5g). IPA analysis of late pattern rod data similarly identified many of the same immune-related pathways implicated in early pattern rod data, including IL-family cytokines. New terms included prolactin, CNTF, and GM-CSF signaling (Supplementary Fig. 15c). The late pattern rod network had fewer nodes than the early network and was centered on IL-6 (Fig. 5h). Late pattern bipolar IPA terms also shared many immune-related terms with early pattern data. Additional terms included CD40, granzyme B, and TNFR signaling (Supp. Fig. 15d). The late pattern bipolar network was centered on interferon regulatory factor 7 (IRF7, Fig. 5i). Finally, a deep literature search was conducted on the top ~50-60 DEGs in each coordinated pattern for each paradigm. More specifically, given the importance of the immune system in regulating retinal regeneration in our NTR-rod model previously[38,57], we asked whether genes had previously been linked to immune response or retinal regeneration (Supp. Fig. 16a). In total, we found that ~38 and ~44% of the top DEGs had been linked to immune system function in the rod and bipolar paradigms, respectively. In terms of cell or tissue regeneration, ~27% of the DEGs from both paradigms had been linked to regeneration in prior studies (Supp. Fig. 16b).

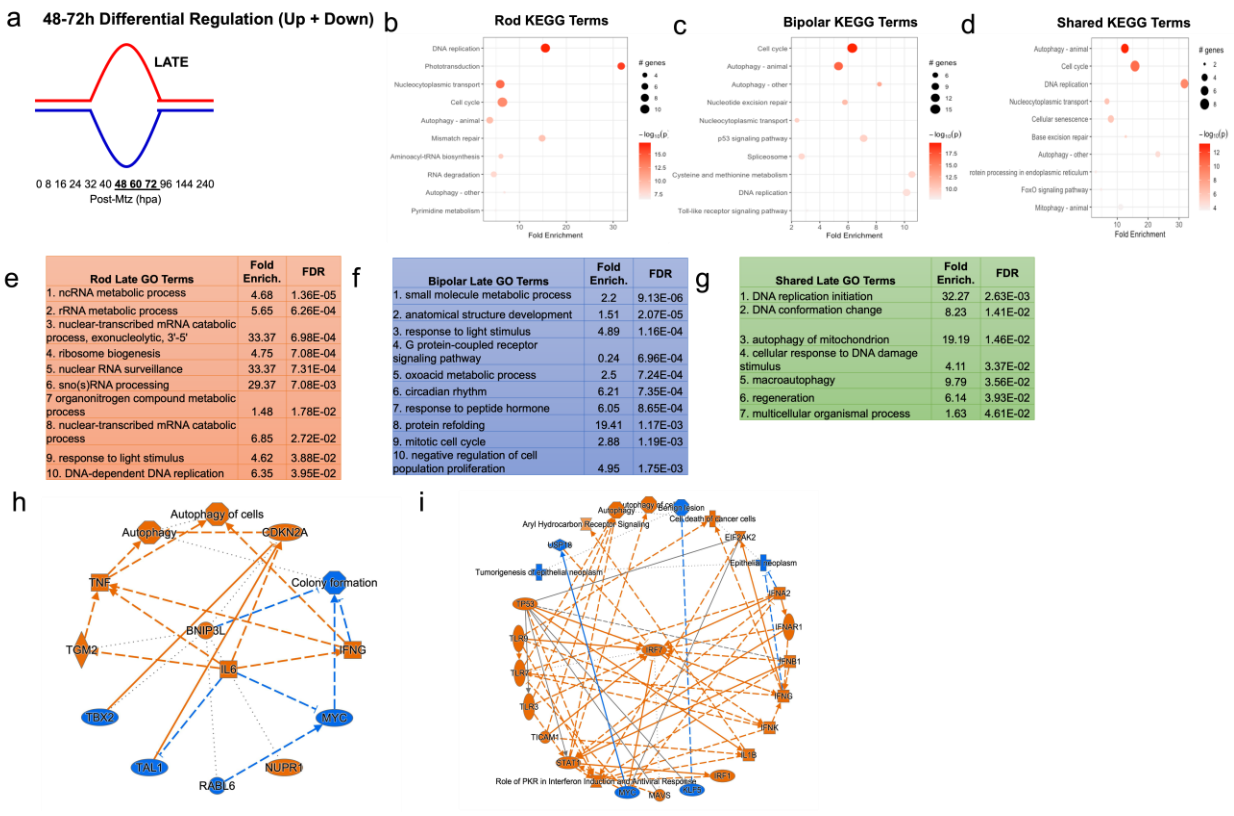

Rod Late GO Terms	Fold Enrich.	FDR
1. ncRNA metabolic process	4.68	1.36E-05
2. rRNA metabolic process	5.65	6.26E-04
3. nuclear-transcribed mRNA catabolic process, exonucleolytic, 3'-5'	33.37	6.98E-04
4. ribosome biogenesis	4.75	7.08E-04
5. nuclear RNA surveillance	33.37	7.31E-04
6. sno(s)RNA processing	29.37	7.08E-03
7 organonitrogen compound metabolic process	1.48	1.78E-02
8. nuclear-transcribed mRNA catabolic process	6.85	2.72E-02
9. response to light stimulus	4.62	3.88E-02
10. DNA-dependent DNA replication	6.35	3.95E-02

Bipolar Late GO Terms	Fold Enrich.	FDR
1. small molecule metabolic process	2.2	9.13E-06
2. anatomical structure development	1.51	2.07E-05
3. response to light stimulus	4.89	1.16E-04
4. G protein-coupled receptor signaling pathway	0.24	6.96E-04
5. oxoacid metabolic process	2.5	7.24E-04
6. circadian rhythm	6.21	7.35E-04
7. response to peptide hormone	6.05	8.65E-04
8. protein refolding	19.41	1.17E-03
9. mitotic cell cycle	2.88	1.19E-03
10. negative regulation of cell population proliferation	4.95	1.75E-03

Shared Late GO Terms	Fold Enrich.	FDR
1. DNA replication initiation	32.27	2.63E-03
2. DNA conformation change	8.23	1.41E-02
3. autophagy of mitochondrion	19.19	1.46E-02
4. cellular response to DNA damage stimulus	4.11	3.37E-02
5. macroautophagy	9.79	3.56E-02
6. regeneration	6.14	3.93E-02
7. multicellular organismal process	1.63	4.61E-02

Fig. 5. Pathway analysis of late DEG pattern in both paradigms.

(a) Curve demonstrating expression pattern for late upregulated (red) and downregulated (blue) genes along our timepoints.

(b-d) Top 10 enriched KEGG pathway terms including p-value and # of genes found as DEGs in the NTR-rod (b), NTR-bipolar (c) or from shared DEGs across both paradigms (d).

(e-g) Top 10 enriched Gene Ontology pathway terms including fold enrichment and false discovery rate in the NTR-rod (e), NTR-bipolar (f) or from shared DEGs across both paradigms (g, only 7 terms enriched in this group).

(h-i) Unsupervised gene networks produced from ingenuity pathway analysis for DEGs in the NTR-rod (h) and NTR-bipolar (i) paradigm. Orange indicates upregulated gene/pathway term while blue indicates downregulated.

a

NTR-Rod	# genes searched	# Immune role	% Immune role	# Regeneration role	Regeneration role %
Early UP	55	30	54.5	20	36.4
EARLY DOWN	61	18	29.5	10	16.4
LATE UP	62	37	59.7	23	37.1
LATE DOWN	61	11	18.0	6	9.8

b

NTR-Bipolar	# genes searched	# Immune role	% Immune role	# Regeneration role	Regeneration role %
Early UP	64	24	37.5	15	23.4
EARLY DOWN	58	15	25.9	11	19.0
LATE UP	53	24	45.3	17	32.1
LATE DOWN	53	12	22.6	12	22.6

c

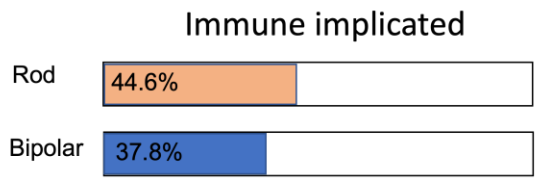

d

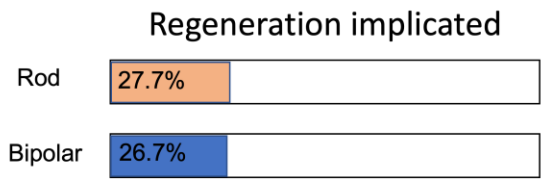

Supp. Fig. 16. Literature search for immune or regeneration related terms.

(a-b) The top ~50-60 DEGs for the NTR-rod (a) and NTR-bipolar (b) patterns were searched in the literature for any links to a role in the immune system or in regeneration. The percentage of those with a link to each term are shown.

(c-d) Bar showing the percentage of top DEGs that were implicated in the immune system (c) or regeneration (d).

Discussion

Promotion of retinal regeneration would provide a transformative therapeutic approach for patients with blinding degenerative diseases. Studies in zebrafish have identified several genes that regulate MG-derived retinal regeneration: *ascl1a*[58], *lin-28 homolog A* [8,11], *sry-box*

transcription factor 2[59], *stat3*[60] as well as multiple gene networks coordinating MG states, including rest, reactivity and proliferation in response to retinal damage[29]. Moreover, overexpression of neurogenic factors such as *ascl1*[4,5,7], and knockdown of inhibitory factors such as the *nfi* genes[29] in MG has been shown to promote limited regenerative responses in the mammalian retina. The neuronal cell types generated with these methods have been predominantly limited to bipolar cells[30], thus not yet well matched to the cell types lost. However, inroads into producing disease-relevant cell types such as retinal ganglion cells has recently been made[7,61]. Further insights into the mechanisms regulating retinal regeneration in fish, bird, and frog species may therefore help to promote the full regenerative potential of the mammalian retina.

Retinal regeneration studies in zebrafish often involve widespread injuries that incur the loss of multiple retinal cell types. Conversely, retinal degenerative diseases such as retinitis pigmentosa typically involve the loss of specific cell types[62]. Following widespread retinal damage the regenerative process largely mirrors retinal development, producing all retinal cell types and involving many factors that also regulate retinogenesis[3,12,12]. Conversely, selective retinal cell ablation paradigms have been associated with novel “fate-biased” regenerative processes, where newly generated cell fates favor the cell type that was lost[13–16]. The mechanisms regulating fate-biased regeneration remain largely unexplored. To begin to address this knowledge, we investigated transcriptomic responses to the selective loss of two retinal cell types, rod photoreceptors and bipolar interneurons.

We first characterized NTR-rod and NTR-bipolar transgenic lines following prodrug-induced cell loss, confirming the specificity of cell loss and quantifying proliferative response in the INL and ONL (Fig. 1). The latter assay was particularly important as prior studies had shown that the extent of rod cell loss impacts how two distinct stem/progenitor cell populations respond; low rod loss leading to rod-committed progenitor proliferation in the ONL only, while extensive rod loss triggered both MG and ONL progenitor proliferation[47]. Our data showed that treating rod-NTR larvae with 10 mM Mtz initiated proliferative responses in both the INL and ONL (Fig. 1l). As expected, bipolar cell ablation elicited cell division in the INL, suggesting both paradigms trigger MG proliferation. Thus, differences in gene expression observed between these paradigms cannot be explained solely by differential stem cell responses, e.g., activation of only rod-committed progenitors in the ONL for the NTR-rod paradigm, though this is clearly a fundamental difference between these paradigms.

To comprehensively characterize transcriptomic changes during rod and bipolar cell regeneration, samples were collected across 12 time points encompassing cell loss and replacement for both paradigms (Fig. 2a). Prior microarray studies have successfully identified genes associated with MG activation [63] and networks activated following various retinal injury paradigms[60,64–68]. For instance, Kassen *et. al* characterized transcriptomic changes triggered by light-induced pan-photoreceptor loss through early regeneration in the adult retina[66]. More recently, Hoang et al., used single-cell RNAseq (scRNA-seq) and single-cell ATAC-seq (Assay for Transposase-Accessible Chromatin) to compare light and NMDA induced retinal cell ablation paradigms during early phases of the regenerative process[29]. Here, by expanding the number of time points analyzed compared to prior studies, we sought to identify genes/pathways

associated with: 1) inflammation and immune cell activation, 2) stem cell activation and dedifferentiation, 3) stem/progenitor cell proliferation, and 4) differentiation of newly generated neurons. We emphasized early time points (every 8 hr from 0-48 h) in an effort to isolate genes linked to the initiation of fate-biased regenerative processes. A total of 364 shared, 918 rod-specific, and 1249 bipolar-specific DEGs were identified (Fig. 2b). Volcano plots and KEGG pathway analysis were used to assess DEGs implicated at each timepoint (Supp. Figs. 4-14). GO, KEGG (via pathfindR), and IPA analysis tools were used to assess DEG subsets exhibiting broadly correlated gene expression patterns (Fig. 3-5). Shared DEGs/pathways were limited more to early time points, while paradigm-specific DEGs/pathways were identified throughout the time course of the study. The number of DEGs diminished for both cell-types starting at 72 hpa. That paradigm-specific DEGs predominated supports previous data suggesting targeted cell ablation elicits a novel fate biased regenerative process[13–16] as opposed to the developmental regeneration commonly associated with widespread retinal cell loss [3,11,12]. Notably, the notion that "regeneration recapitulates development" was also refuted in the recent scRNA-seq/ATAC-seq study by Hoang et al. where the majority of DEGs during MG reprogramming were implicated in development, but most of them showed inverse expression patterns compared to developmental time frames (e.g. if they increase in expression through retinal development they typically decrease in expression following injury)[29].

KEGG pathway analysis per each timepoint identified previously implicated pathways (e.g., mTor, Notch, and Wnt signaling)[8,54,65,69,70], and terms linked to the regulation of stem cell function but not previously associated with retinal regeneration (e.g., glutathione metabolism[71], FoxO signaling[72], and cellular senescence[73]). However, the number of genes and fold-enrichment

were not particularly robust for data from individual timepoints. To enhance pathway analyses, we grouped DEGs into four coordinately regulated sets for each paradigm: up or down early (16-32 hr) and up or down late (48-72 hr, Figs. 3a,b). Notably, this accounted for the majority of DEGs and reinforced that paradigm-specific DEGs outnumbered shared DEGs (Fig. 3c). Representative genes in the early up group for the rod paradigm included known factors (e.g., *activating transcription factor 3- atf3*, *stat3*)[60,74] and genes not previously associated with retinal regeneration (e.g., *glutathione S-transferase pi 1- gstp1*). Among the known set, factors associated with immune system reactivity were prevalent, including a number of genes previously shown to be upregulated in MG at 16h post light ablation in adult zebrafish[60] (e.g., *janus kinase 1- jak1*, *stat3*, *suppression of cytokine signaling 3b- socs3b*, *cytokine inducible SH2-containing protein- cish*, *irf9* and *complement component 7b- c7b*). GO analysis additionally identified shared late pattern enrichment for the broad term "regeneration" based on the differential regulation of the genes *annexin A1a- anxa1a*, *ubiquitin-like with PHD and ring finger domains 1- uhrf1*, *socs3a*, *capthespin Ba- ctsba*, *legumain- lgmn*, *major vault protein-mvp*, *v-fos FBJ murine osteosarcoma viral oncogene homolog Ab- fosab*, and *GLIS family zinc finger 3- glis3* (Fig. 5g).

Next, IPA was used to reveal differential regulation of pathways at early and late stages of regeneration in each model. For both cell types, and at both early and late timepoints, multiple shared and unique immune-related pathways were identified, e.g., cytokines, Jak/Stat, Toll-like receptor and prolactin signaling (Supp. Fig. 15). We then produced unsupervised DEG networks using the coordinated expression pattern data, i.e., rod-early, rod-late, bipolar-early and bipolar-late. Known pro-regenerative and pro-inflammatory factors STAT3 and IL-6[60,75] were identified

as central mediators in the rod paradigm (Fig. 4h, 5h), while PPARG and IRF7 were implicated as central mediators for the bipolar paradigm (Fig. 4i, 5i). PPARG has recently been tied to zebrafish retinal progenitor cell function in adults through interactions with metabolic pathways.[76] Interestingly, IRF7 has been implicated as a key regulator of microglia reactivity, its upregulation promoting a phenotypic switch from an inflammatory to anti-inflammatory state, aka stimulating resolution of microglia activation[77,78]. Our prior work suggested that accelerating the resolution process by exposure to the immunosuppressant dexamethasone 24 hrs after induction of rod cell ablation led to enhanced rod cell regeneration in zebrafish[57]. Together, these studies implicate induction of IRF7 expression as potential strategy for promoting neuronal regeneration.

Both IL-6 and interferons activate JAK/STAT signaling[75,79], a known mediator of the response to retinal damage[60] regulating cell migration[80], proliferation[60], apoptosis[81], immune system[82] and oxidative stress[83] responses. DEGs in the JAK/STAT family were primarily upregulated in the rod (e.g, *stat3, jak1, cish, socs1a/3a/3b*) and bipolar paradigms (e.g, *cish, socs1a/3a/3b, stat1a/1b/25a/5b*). However, the specific JAK/STAT family members involved differed between our two paradigms (e.g., *stat3* for rod and *stat1a/b and stat2* for bipolar). Similarly, different cell death pathways were also implicated, NTR-rod being linked to necroptosis (Fig. 4b) while NTR-bipolar was linked to apoptosis (Fig. 4c, f), These findings align with a recent drug screen in the same NTR-rod model where inhibitors and genetic disruption of parthanatos and necroptosis protected rods from cell death while inhibition of apoptosis did not[40]. Interestingly, recent work in multiple mouse tumor models links necroptotic signaling to the activation of IL-6 and Stat3[84–86] while apoptotic signaling was linked to Stat5 activation[87], matching gene expression and cell

death patterns in our models. JAK/STAT signaling receives feedback inhibition from Suppression of Cytokine Signaling (SOCS) genes[88]. Notably, ablation of both cell types was followed by upregulation of *socs3a*, *socs3b*, *socs1a* and *cish*. *Socs3a* has been implicated as a mediator of hair and liver cell regeneration in zebrafish through activation of resident stem cells and progenitor differentiation[89,90], respectively. In the zebrafish retina, *socs3a* expression is upregulated following optic nerve injury, where it is thought to inhibit axonal regrowth[91]. as well as strongly upregulated in an adult zebrafish photoreceptor lesion model[66]. Finally, the Reh lab has recently shown that combining overexpression of *ascl1* with inhibition of STAT signaling stimulates enhanced MG-derived regeneration in the mouse retina[30]. Here, *socs1a*, *socs3a/b* and *cish* likely serve to similarly limit over-activation of JAK/STAT signaling during retinal regeneration following activation of distinct STATs. These results highlight how cell-specific regulation of family members within a given signaling pathway may delineate fate-biased from shared (i.e., developmental) regenerative mechanisms. By extension, further insights into the regulation of fate-biased regenerative mechanisms will likely aid in the development of cell-type targeted therapeutic strategies to restore vision.

Materials and Methods

Aquaculture

Zebrafish were maintained under standard environmental conditions (~28°C, 14hr:10hr light:dark cycle) under an approved ACUC animal use protocol. Larvae were fed paramecia starting at 5 days post-fertilization (dpf), then paramecia and *Artemia salina* from 9-16 dpf. Late stage larvae (e.g., 8 dpf) slated for imaging were kept in 12 well plates in 5 ml of system water until 12 dpf after which they were sacrificed.

Transgenic Lines

A bipartite Gal4/UAS [92] transgenic zebrafish line derived with a 1,482 bp promoter element from the *nyctalopin* (*nyx*) gene [93,94], *Tg(nyx:Gal4-VP16)q16a*, and a Gal4-driven reporter, *(UAS:GAP-YFP)q16b*, expresses membrane-tagged yellow fluorescent protein (YFP) in a subpopulation of bipolar cells [48]. Crosses to a UAS-reporter/effector line facilitating prodrug-induced cell ablation, *Tg(UAS-E1b:NfsB-mCherry)c264* [95], resulted in triple transgenic fish expressing an NTR-mCherry fusion protein in subsets of *nyx*-promoter targeted bipolar cells (*q16a;q16b;c264*; hereafter, NTR-bipolar lines). A transgenic line derived with a 3.7 kb promoter element from the *rhodopsin (rho)* gene (kind gift of Dr. Shoji Kawamura) [49] expresses a YFP-NTR fusion protein in rod photoreceptor cells, *Tg(rho:YFP-Eco.NfsB)gmc500* [46] (hereafter, NTR-rod lines). Retinal morphology was monitored during imaging studies by crossing both NTR lines with *Tg(pax6-DF4:gap43-CFP)q01* which expresses membrane tagged CFP throughout the retina (see Fig. 1A-B) [96]. Transgenic fish were propagated in the *roy orbison* (aka, $mpv17^{a9/a9}$, hereafter $roy^{a9/a9}$)[97,98] pigmentation mutant background to facilitate intravital imaging [99]. However, for differential gene expression studies, to minimize expression variance due to differences in transgene copy number, outcrosses to an AB wildtype strain (WT) were performed to generate heterozygotes.

Mtz Treatment

For histological experiments, *in vivo* imaging experiments and all microarray tissue collections, transgenic NTR-bipolar and NTR-rod larvae were screened and separated into two equal sized groups at 6 dpf: 1) non-treated controls (Cntl); and 2) those treated with 10mM Mtz for 24 hr to induce cell death, from 6-7 dpf (or DMSO-treated controls where applicable). After Mtz treatment, fish were rinsed into system water and fed paramecia until sacrificed.

mRNA Isolation and Preparation

Whole eye mRNA was prepared across twelve time points: t0 (just prior to Mtz exposure); t8, t16, and t24 hr (during Mtz treatment); and t32, t40, t48, t60, t72, t96, t144, and t240 hr (after Mtz removal during recovery (Fig. 2A). Sample collection started at 8:00 a.m. on the day larvae reached 6 dpf. At each time point, 16 eyes from 8 larvae were isolated per condition. To isolate eyes, larvae were euthanized in 0.4% tricaine for 5 mins followed by cervical transection. Whole eye pairs were manually isolated under an Olympus SZX16 epifluorescence stereoscope and immediately placed into a chilled/sterile 1.5 ml tube with 50 µl of TriZOL (Life Technologies); samples were then stored at -80°C until extraction. This protocol was followed for three biological repeats per condition/time point for NTR-rod and NTR-bipolar lines. Samples were batch extracted and processed following the final time. All samples were processed in the Medical College of Georgia (MCG, former Mumm lab location) Integrated Genomics Core for mRNA isolation, cDNA library construction, and microarray hybridization.

Microarrays

GeneChip Zebrafish Genome Microarrays (Affymetrix) were processed by the MCG Genomic Core. Each run involved sibling zebrafish and consisted of 23 RNA samples across each regenerative paradigm—1 pretreatment, and 11 time points from the control and Mtz treatment groups. RNA sample quality was assessed by concentration and the RNA Integrity Number (RIN), an algorithm that assigns integrity values to RNA measurements [100]. Only samples attaining a minimal concentration of ≥100ng/µL (5µL total) and a RNA integrity number (RIN) value of ≥8 were used for microarray hybridizations [100]. Runs where a minimum of 21 of 23 samples were deemed of good quality were utilized in the microarray studies. Three runs were

processed per regenerative paradigm resulting in six microarray sets (Supplementary Table 1) and a total 138 microarrays overall.

Tissue preparation and immunohistochemistry

For immunohistochemistry, larval zebrafish were euthanized, fixed in 4% paraformaldehyde (PFA) for 8 hr, washed three times in 1x PBS (phosphate buffered saline; EMD Millipore) for 30 min and stored at 4°C. Samples were mounted in cryogel embedding medium within the next 2-4 days, frozen in liquid nitrogen then stored at -80^{0}C until sectioned in the lateral plane at 25 μm thickness with a cryostat. Sliced sections were collected on standard microscope slides and stored at 4°C.

For immunolabeling, slides were air dried at room temperature for ~1 hr, rinsed in 1xPBS and then re-fixed with 4% PFA for 15 min. PBST rinses (1xPBS +0.1% Tween20, Fisher Scientific) were conducted to remove trace PFA followed by 5 min antigen retrieval with SDS (1% Sodium Dodecyl Sulfate; Fisher Scientific) in PBS. The blocking phase was performed with 3% goat serum in PBDT (1xPBS, 1% BSA, 1% DMSO, 0.1% TritonX-100) for 30 min and incubated with primary antibody/1% goat serum/PBDT overnight at 4°C. The next morning, slides were rinsed in PBST, stained with secondary antibody/PBDT ~1 hr in a light protected humidity chamber and cover-slipped (22x50 mm, Fisher Scientific). PBST rinses removed unbound secondary antibody. Samples were protected with Vectashield + DAPI (Vector Laboratories) and cover-slipped (24x50 mm, Fisher Scientific).

Primary antibodies included: mouse anti-PCNA monoclonal antibody (1:1000, clone PC10; Sigma Aldrich), rabbit anti-Caspase-3 monoclonal antibody (1:500, clone C92-605; BD Biosciences), Click-iT Tunel Alexa Fluor 647 (1:500; Life Technologies), mouse anti-zpr-1 monoclonal antibody (1:750; ZIRC), mouse anti-zpr-3 monoclonal antibody (1:750; ZIRC),

mouse anti-ZS-4 monoclonal antibody (1:750; ZIRC). Secondary antibodies included: anti-mouse Alexa Fluor 430 (1:500; Life Technologies), anti-mouse Alexa Fluor 635 (1:500; Life Technologies), anti-rabbit Alexa Fluor 430 (1:500; Life Technologies).

Cell Counting and Analysis

Images were collected with an Olympus FV1000 Confocal Microscope (405, 440, 488, 515, 559, and 635nm laser lines). Stacked confocal images were obtained using a 40x oil immersion objective with a 2.5 µm step size, 130 µm aperture, and 10 µm total depth. Five sections were collected per retina centered around the optic nerve. Images (Olympus .OIB format) were analyzed using ImageJ. Manual cell counts were averaged across sections per retina and averaged within each group. Student's t-test and One-way ANOVA were used for statistical comparisons between groups.

Sample Quality and Differential Expression Analysis

Data were collected from 138 Genechip Zebrafish Genome arrays (Affymetrix) across four conditions: NTR-rod cntrl, NTR-rod Mtz, NTR-bipolar cntrl, and NTR-bipolar Mtz. The Bioconductor suite in the R statistical software [101], LIMMA [102], Carmaweb [103], and Microsoft Access were used for data processing, differential expression testing and storage. Prior to statistical analysis, Robust Multi-array Average (RMA) pre-processing routine [104] and Quality control assessments [105] were used for background correction, normalization and quality control. A set of differentially expressed genes was derived using LIMMA with a false discovery rate adjusted p-value of 0.05. Differentially expressed genes were defined as those expressing a 1.5-fold up or downregulation at any time point in regeneration. Pathway analysis was performed using Ingenuity Pathway Analysis (IPA), Gene Ontology (GO) and KEGG pathway analysis (via

the pathfindR R studio package). An adjusted p value below 0.05 was used throughout as a cutoff for significance.

qPCR Processing

Extracted mRNA samples were reverse transcribed (Qiagen Omniscript RT kit, Qiagen) and stored at -20°C. Samples were run in triplicate using the BioRad iQ SYBR Green Supermix (BioRad) in iCycler IQ 96 well PCR plates (Bio-Rad) on a BioRad iCycler equipped with an iCycler iQ Detection System. The protocol consisted of three phases: 1) 92˚C for 10:00 min, 2) 50x 92˚C for 00:15 min, 60˚C for 01:00 min, 3) 81x 55˚c→95˚c for 00:10 min. β-actin served as the house keeping gene and $2^{-\Delta\Delta CT}$ method was used for normalization to ensure equal amounts of cDNA for comparisons. qPCR primers were designed using the online tool QuantPrime.

References

1. Too, L. K. & Simunovic, M. P. Retinal Stem/Progenitor Cells Derived From Adult Müller Glia for the Treatment of Retinal Degeneration. *Front. Cell Dev. Biol.* **9**, 749131 (2021).
2. Lahne, M., Nagashima, M., Hyde, D. R. & Hitchcock, P. F. Reprogramming Müller Glia to Regenerate Retinal Neurons. *Annu. Rev. Vis. Sci.* **6**, 171–193 (2020).
3. Lenkowski, J. R. & Raymond, P. A. Müller glia: Stem cells for generation and regeneration of retinal neurons in teleost fish. *Prog. Retin. Eye Res.* **40**, 94–123 (2014).
4. Ueki, Y. *et al.* Transgenic expression of the proneural transcription factor Ascl1 in Müller glia stimulates retinal regeneration in young mice. *Proc. Natl. Acad. Sci. U. S. A.* **112**, 13717–13722 (2015).
5. Jorstad, N. L. *et al.* Stimulation of functional neuronal regeneration from Müller glia in adult mice. *Nature* **548**, 103–107 (2017).

6. Jorstad, N. L. *et al.* STAT Signaling Modifies Ascl1 Chromatin Binding and Limits Neural Regeneration from Muller Glia in Adult Mouse Retina. *Cell Rep.* **30**, 2195-2208.e5 (2020).
7. Todd, L. *et al.* Efficient stimulation of retinal regeneration from Müller glia in adult mice using combinations of proneural bHLH transcription factors. *Cell Rep.* **37**, 109857 (2021).
8. Yao, K. *et al.* Wnt regulates proliferation and neurogenic potential of Müller glial cells through a Lin28/let-7 miRNA-dependent pathway in adult mammalian retina. *Cell Rep.* **17**, 165–178 (2016).
9. Goldman, D. Müller glial cell reprogramming and retina regeneration. *Nat. Rev. Neurosci.* **15**, 431–442 (2014).
10. Gorsuch, R. a & Hyde, D. R. Regulation of Müller glial dependent neuronal regeneration in the damaged adult zebrafish retina. *Exp. Eye Res.* **123**, 131–40 (2014).
11. Elsaeidi, F. *et al.* Notch suppression collaborates with Ascl1 and Lin28 to unleash a regenerative response in fish retina, but not in mice. *J. Neurosci.* (2018) doi:10.1523/JNEUROSCI.2126-17.2018.
12. Lahne, M., Brecker, M., Jones, S. E. & Hyde, D. R. The Regenerating Adult Zebrafish Retina Recapitulates Developmental Fate Specification Programs. *Front. Cell Dev. Biol.* **8**, 617923 (2020).
13. Fraser, B., DuVal, M. G., Wang, H. & Allison, W. T. Regeneration of Cone Photoreceptors when Cell Ablation Is Primarily Restricted to a Particular Cone Subtype. *PLoS ONE* (2013) doi:10.1371/journal.pone.0055410.
14. D'Orazi, F. D., Suzuki, S. C., Darling, N., Wong, R. O. & Yoshimatsu, T. Conditional and biased regeneration of cone photoreceptor types in the zebrafish retina. *J. Comp. Neurol.* (2020) doi:10.1002/cne.24933.

15. Ng Chi Kei, J., Currie, P. D. & Jusuf, P. R. Fate bias during neural regeneration adjusts dynamically without recapitulating developmental fate progression. *Neural Develop.* (2017) doi:10.1186/s13064-017-0089-y.

16. DuVal, M. G. & Allison, W. T. Impacts of the retinal environment and photoreceptor type on functional regeneration. *Neural Regeneration Research* (2017) doi:10.4103/1673-5374.202930.

17. Braisted, J. E., Essman, T. F. & Raymond, P. a. Selective regeneration of photoreceptors in goldfish retina. *Dev. Camb. Engl.* **120**, 2409–19 (1994).

18. Vihtelic, T. S. & Hyde, D. R. Light-Induced Rod and Cone Cell Death and Regeneration in the Adult albino Zebrafish (Danio rerio) Retina ABSTRACT : (2000).

19. Thomas, J. L., Nelson, C. M., Luo, X., Hyde, D. R. & Thummel, R. Characterization of multiple light damage paradigms reveals regional differences in photoreceptor loss. *Exp. Eye Res.* (2012) doi:10.1016/j.exer.2012.02.004.

20. Thomas, J. L. & Thummel, R. A novel light damage paradigm for use in retinal regeneration studies in adult zebrafish. *J. Vis. Exp. JoVE* (2013).

21. Maier, W. & Wolburg, H. Regeneration of the Goldfish Retina After Exposure to Different Doses of Ouabain. *Cell Tissue Res.* **118**, 99–118 (1979).

22. Fimbel, S. M., Montgomery, J. E., Burket, C. T. & Hyde, D. R. Regeneration of inner retinal neurons after intravitreal injection of ouabain in zebrafish. *J. Neurosci. Off. J. Soc. Neurosci.* **27**, 1712–24 (2007).

23. Hitchcock, P. F., Lindsey Myhr, K. J., Easter, S. S., Mangione-Smith, R. & Jones, D. D. Local regeneration in the retina of the goldfish. *J. Neurobiol.* **23**, 187–203 (1992).

24. Cameron, D. a & Easter, S. S. Cone photoreceptor regeneration in adult fish retina: phenotypic determination and mosaic pattern formation. *J. Neurosci. Off. J. Soc. Neurosci.* **15**, 2255–71 (1995).

25. Johns, P. R. & Fernald, R. D. Genesis of rods in teleost fish retina. *Nature* (1981) doi:10.1038/293141a0.

26. Raymond, P. A. & Rivlin, P. K. Germinal cells in the goldfish retina that produce rod photoreceptors. *Dev. Biol.* (1987) doi:10.1016/0012-1606(87)90338-1.

27. Wu, D. M. *et al.* Cones regenerate from retinal stem cells sequestered in the inner nuclear layer of adult goldfish retina. *Invest. Ophthalmol. Vis. Sci.* **42**, 2115–24 (2001).

28. Hitchcock, P. F. & Raymond, P. A. The Teleost Retina as a Model for Developmental and Regeneration Biology. *Zebrafish* (2004) doi:10.1089/zeb.2004.1.257.

29. Hoang, T. *et al.* Gene regulatory networks controlling vertebrate retinal regeneration. *Science* **370**, (2020).

30. Jorstad, N. L. *et al.* Stimulation of functional neuronal regeneration from Müller glia in adult mice. *Nature* (2017) doi:10.1038/nature23283.

31. Anlezark, G. M. *et al.* The bioactivation of 5-(aziridin-1-yl)-2,4-dinitrobenzamide (CB1954)--I. Purification and properties of a nitroreductase enzyme from Escherichia coli--a potential enzyme for antibody-directed enzyme prodrug therapy (ADEPT). *Biochem. Pharmacol.* **44**, 2289–95 (1992).

32. Knox, R. J., Friedlos, F., Sherwood, R. F., Melton, R. G. & Anlezark, G. M. The bioactivation of 5-(aziridin-1-yl)-2,4-dinitrobenzamide (CB1954)--II. A comparison of an Escherichia coli nitroreductase and Walker DT diaphorase. *Biochem. Pharmacol.* **44**, 2297–301 (1992).

33. Sunters, A., Baer, J. & Bagshawe, K. D. Cytotoxicity and activation of CB1954 in a human tumour cell line. *Biochem. Pharmacol.* **41**, 1293–8 (1991).

34. Williams, E. M. *et al.* Nitroreductase gene-directed enzyme prodrug therapy: insights and advances toward clinical utility. *Biochem. J.* **471**, 131–153 (2015).

35. Bridgewater, J. A. *et al.* Expression of the bacterial nitroreductase enzyme in mammalian cells renders them selectively sensitive to killing by the prodrug CB1954. *Eur. J. Cancer Oxf. Engl. 1990* **31A**, 2362–2370 (1995).

36. White, D. T. & Mumm, J. S. The nitroreductase system of inducible targeted ablation facilitates cell-specific regenerative studies in zebrafish. *Methods* **62**, 232–240 (2013).

37. Mathias, J. R., Zhang, Z., Saxena, M. T. & Mumm, J. S. Enhanced cell-specific ablation in zebrafish using a triple mutant of escherichia coli nitroreductase. *Zebrafish* (2014) doi:10.1089/zeb.2013.0937.

38. White, D. T. *et al.* Immunomodulation-accelerated neuronal regeneration following selective rod photoreceptor cell ablation in the zebrafish retina. *Proc. Natl. Acad. Sci. U. S. A.* (2017) doi:10.1073/pnas.1617721114.

39. White, D. T. *et al.* ARQiv-HTS, a versatile whole-organism screening platform enabling in vivo drug discovery at high-throughput rates. *Nat. Protoc.* **11**, 2432–2453 (2016).

40. Zhang, L. *et al.* Large-scale phenotypic drug screen identifies neuroprotectants in zebrafish and mouse models of retinitis pigmentosa. *eLife* **10**, e57245 (2021).

41. Sharrock, A. V. *et al.* NTR 2.0: a rationally engineered prodrug-converting enzyme with substantially enhanced efficacy for targeted cell ablation. *Nat. Methods* **19**, 205–215 (2022).

42. Curado, S. *et al.* Conditional targeted cell ablation in zebrafish: A new tool for regeneration studies. *Dev. Dyn.* (2007) doi:10.1002/dvdy.21100.

43. Pisharath, H., Rhee, J. M., Swanson, M. a, Leach, S. D. & Parsons, M. J. Targeted ablation of beta cells in the embryonic zebrafish pancreas using E. coli nitroreductase. *Mech. Dev.* **124**, 218–29 (2007).

44. Perkins, B. D. Zebrafish models of inherited retinal dystrophies. *J. Transl. Genet. Genomics* **6**, 95–110 (2022).

45. Ariga, J., Walker, S. L. & Mumm, J. S. Multicolor time-lapse imaging of transgenic zebrafish: visualizing retinal stem cells activated by targeted neuronal cell ablation. *J. Vis. Exp. JoVE* 2–7 (2010) doi:10.3791/2093.

46. Walker, S. L. *et al.* Automated reporter quantification in vivo: High-throughput screening method for reporter-based assays in zebrafish. *PLoS ONE* **7**, e29916 (2012).

47. Montgomery, J. E., Parsons, M. J. & Hyde, D. R. A novel model of retinal ablation demonstrates that the extent of rod cell death regulates the origin of the regenerated zebrafish rod photoreceptors. *J. Comp. Neurol.* **518**, 800–814 (2010).

48. Schroeter, E. H., Wong, R. O. L. & Gregg, R. G. In vivo development of retinal ON-bipolar cell axonal terminals visualized in nyx::MYFP transgenic zebrafish. *Vis. Neurosci.* **23**, 833–43 (2006).

49. Hamaoka, T., Takechi, M., Chinen, A., Nishiwaki, Y. & Kawamura, S. Visualization of rod photoreceptor development using GFP-transgenic zebrafish. *Genesis* **34**, 215–20 (2002).

50. Schmitt, E. A. & Dowling, J. E. Comparison of topographical patterns of ganglion and photoreceptor cell differentiation in the retina of the zebrafish, Danio rerio. *J. Comp. Neurol.* (1996) doi:10.1002/(SICI)1096-9861(19960722)371:2<222::AID-CNE3>3.0.CO;2-4.

51. Larison, K. D. & Bremiller, R. Early onset of phenotype and cell patterning in the embryonic zebrafish retina. *Development* (1990).

52. Vihtelic, T. S., Doro, C. J. & Hyde, D. R. Cloning and characterization of six zebrafish photoreceptor opsin cDNAs and immunolocalization of their corresponding proteins. *Vis. Neurosci.* (1999) doi:10.1017/S0952523899163168.

53. Gavrieli, Y., Sherman, Y. & Ben-Sasson, S. A. Identification of programmed cell death in situ via specific labeling of nuclear DNA fragmentation. *J. Cell Biol.* (1992) doi:10.1083/jcb.119.3.493.

54. Meyers, J. R. *et al.* β-catenin/Wnt signaling controls progenitor fate in the developing and regenerating zebrafish retina. *Neural Develop.* **7**, 30 (2012).

55. Smith, C. J. & Osborn, A. M. Advantages and limitations of quantitative PCR (Q-PCR)-based approaches in microbial ecology. *FEMS Microbiol. Ecol.* **67**, 6–20 (2009).

56. Ulgen, E., Ozisik, O. & Sezerman, O. U. pathfindR: An R Package for Comprehensive Identification of Enriched Pathways in Omics Data Through Active Subnetworks. *Front. Genet.* **10**, 858 (2019).

57. Emmerich, K. B. *et al.* Dendrimer-targeted immunosuppression of microglia reactivity super-accelerates photoreceptor regeneration in the zebrafish retina. *bioRxiv* 2020.08.05.238352 (2021) doi:10.1101/2020.08.05.238352.

58. Fausett, B. V., Gumerson, J. D. & Goldman, D. The proneural basic helix-loop-helix gene Ascl1a is required for retina regeneration. *J. Neurosci.* (2008) doi:10.1523/JNEUROSCI.4853-07.2008.

59. Gorsuch, R. A. *et al.* Sox2 regulates Müller glia reprogramming and proliferation in the regenerating zebrafish retina via Lin28 and Ascl1a. *Exp. Eye Res.* (2017) doi:10.1016/j.exer.2017.05.012.

60. Nelson, C. M. *et al.* Stat3 defines three populations of müller glia and is required for initiating maximal müller glia proliferation in the regenerating zebrafish retina. *J. Comp. Neurol.* (2012) doi:10.1002/cne.23213.

61. Xiao, D. *et al.* Directed robust generation of functional retinal ganglion cells from Müller glia. *bioRxiv* 735357 (2019) doi:10.1101/735357.

62. Dryja, T. P. *et al.* A point mutation of the rhodopsin gene in one form of retinitis pigmentosa. *Nature* (1990) doi:10.1038/343364a0.

63. Sifuentes, C. J., Kim, J. W., Swaroop, A. & Raymond, P. A. Rapid, dynamic activation of Müller Glial stem cell responses in Zebrafish. *Invest. Ophthalmol. Vis. Sci.* **57**, 5148–5160 (2016).

64. Morris, A. C., Forbes-Osborne, M. A., Pillai, L. S. & Fadool, J. M. Microarray analysis of XOPS-mCFP zebrafish retina identifies genes associated with rod photoreceptor degeneration and regeneration. *Invest. Ophthalmol. Vis. Sci.* (2011) doi:10.1167/iovs.10-6022.

65. Yurco, P. & Cameron, D. A. Cellular correlates of proneural and notch-delta gene expression in the regenerating zebrafish retina. *Vis. Neurosci.* **24**, 437–443 (2007).

66. Kassen, S. C. *et al.* Time course analysis of gene expression during light-induced photoreceptor cell death and regeneration in albino zebrafish. *Dev. Neurobiol.* (2007) doi:10.1002/dneu.20362.

67. Ramachandran, R., Zhao, X.-F. & Goldman, D. Insm1a-mediated gene repression is essential for the formation and differentiation of Müller glia-derived progenitors in the injured retina. *Nat. Cell Biol.* **14**, 1013–1023 (2012).

68. Cameron, D. A., Gentile, K. L., Middleton, F. A. & Yurco, P. Gene expression profiles of intact and regenerating zebrafish retina. *Mol. Vis.* **11**, 775–791 (2005).

69. Sahu, A., Devi, S., Jui, J. & Goldman, D. Notch signaling via Hey1 and Id2b regulates Müller glia's regenerative response to retinal injury. *Glia* **69**, 2882–2898 (2021).

70. Zhang, Z. *et al.* Inflammation-induced mammalian target of rapamycin signaling is essential for retina regeneration. *Glia* **68**, 111–127 (2020).

71. Jeong, E. M. *et al.* Real-Time Monitoring of Glutathione in Living Cells Reveals that High Glutathione Levels Are Required to Maintain Stem Cell Function. *Stem Cell Rep.* **10**, 600–614 (2018).

72. Ludikhuize, M. C. & Rodríguez Colman, M. J. Metabolic Regulation of Stem Cells and Differentiation: A Forkhead Box O Transcription Factor Perspective. *Antioxid. Redox Signal.* **34**, 1004–1024 (2021).

73. Ogrodnik, M. *et al.* Obesity-Induced Cellular Senescence Drives Anxiety and Impairs Neurogenesis. *Cell Metab.* **29**, 1233 (2019).

74. Saul, K. E., Koke, J. R. & García, D. M. Activating transcription factor 3 (ATF3) expression in the neural retina and optic nerve of zebrafish during optic nerve regeneration. *Comp. Biochem. Physiol. A. Mol. Integr. Physiol.* **155**, 172–182 (2010).

75. Nakajima, K. *et al.* A central role for Stat3 in IL-6-induced regulation of growth and differentiation in M1 leukemia cells. *EMBO J.* (1996) doi:10.1002/j.1460-2075.1996.tb00734.x.

76. Luzio, A. *et al.* Effects of short-term exposure to genistein and overfeeding diet on the neural and retinal progenitor competence of adult zebrafish (Danio rerio). *Neurotoxicol. Teratol.* **88**, 107030 (2021).

77. Hagemeyer, N. & Prinz, M. Burning down the house: IRF7 makes the difference for microglia. *EMBO J.* **33**, 2885–2886 (2014).

78. Cohen, M. *et al.* Chronic exposure to TGFβ1 regulates myeloid cell inflammatory response in an IRF7-dependent manner. *EMBO J.* **33**, 2906–2921 (2014).

79. Fukada, T. STAT3 orchestrates contradictory signals in cytokine-induced G1 to S cell-cycle transition. *EMBO J.* (1998) doi:10.1093/emboj/17.22.6670.

80. Yamashita, S. *et al.* Stat3 controls cell movements during zebrafish gastrulation. *Dev. Cell* (2002) doi:10.1016/S1534-5807(02)00126-0.

81. Avalle, L., Pensa, S., Regis, G., Novelli, F. & Poli, V. STAT1 and STAT3 in tumorigenesis: A matter of balance. *JAK-STAT* (2012) doi:10.4161/jkst.20045.

82. Hutchins, A. P., Diez, D. & Miranda-Saavedra, D. The IL-10/STAT3-mediated anti-inflammatory response: Recent developments and future challenges. *Brief. Funct. Genomics* (2013) doi:10.1093/bfgp/elt028.

83. Carballo, M. *et al.* Oxidative stress triggers STAT3 tyrosine phosphorylation and nuclear translocation in human lymphocytes. *J. Biol. Chem.* (1999) doi:10.1074/jbc.274.25.17580.

84. Zhao, Q. *et al.* MLKL inhibits intestinal tumorigenesis by suppressing STAT3 signaling pathway. *Int. J. Biol. Sci.* **17**, 869–881 (2021).

85. Zhao, Q. *et al.* RIPK3 Suppresses the Progression of Spontaneous Intestinal Tumorigenesis. *Front. Oncol.* **11**, 664927 (2021).

86. Smith, A. D. *et al.* Autocrine IL6-mediated activation of the STAT3-DNMT axis silences the TNFα-RIP1 necroptosis pathway to sustain survival and accumulation of myeloid-derived suppressor cells. *Cancer Res.* **80**, 3145–3156 (2020).

87. Jiang, L. *et al.* Long non-coding RNA RP11-468E2.5 curtails colorectal cancer cell proliferation and stimulates apoptosis via the JAK/STAT signaling pathway by targeting STAT5 and STAT6. *J. Exp. Clin. Cancer Res. CR* **38**, 465 (2019).

88. Thanasaksiri, K., Hirono, I. & Kondo, H. Identification and expression analysis of suppressors of cytokine signaling (SOCS) of Japanese flounder Paralichthys olivaceus. *Fish Shellfish Immunol.* (2016) doi:10.1016/j.fsi.2016.09.018.

89. Liang, J. *et al.* The stat3/socs3a pathway is a key regulator of hair cell regeneration in zebrafish stat3/socs3a pathway: Regulator of hair cell regeneration. *J. Neurosci.* (2012) doi:10.1523/JNEUROSCI.5785-10.2012.

90. Khaliq, M. *et al.* Stat 3 regulates liver progenitor cell-driven liver regeneration in zebrafish. *Gene Expr.* (2018) doi:10.3727/105221618X15242506133273.

91. Elsaeidi, F., Bemben, M. A., Zhao, X.-F. & Goldman, D. Jak/Stat signaling stimulates zebrafish optic nerve regeneration and overcomes the inhibitory actions of Socs3 and Sfpq. *J. Neurosci. Off. J. Soc. Neurosci.* **34**, 2632–2644 (2014).

92. Köster, R. W. & Fraser, S. E. Tracing transgene expression in living zebrafish embryos. *Dev. Biol.* **233**, 329–46 (2001).

93. Bech-Hansen, N. T. *et al.* Mutations in NYX, encoding the leucine-rich proteoglycan nyctalopin, cause X-linked complete congenital stationary night blindness. *Nat. Genet.* (2000) doi:10.1038/81619.

94. Pusch, C. M. *et al.* The complete form of X-linked congenital stationary night blindness is caused by mutations in a gene encoding a leucine-rich repeat protein. *Nat. Genet.* (2000) doi:10.1038/81627.

95. Davison, J. M. *et al.* Transactivation from Gal4-VP16 transgenic insertions for tissue-specific cell labeling and ablation in zebrafish. *Dev. Biol.* **304**, 811–24 (2007).

96. Godinho, L. *et al.* Targeting of amacrine cell neurites to appropriate synaptic laminae in the developing zebrafish retina. *Development* **132**, 5069–79 (2005).

97. D'Agati, G. *et al.* A defect in the mitochondrial protein Mpv17 underlies the transparent casper zebrafish. *Dev. Biol.* **430**, 11–17 (2017).

98. Ren, J. Q., McCarthy, W. R., Zhang, H., Adolph, A. R. & Li, L. Behavioral visual responses of wild-type and hypopigmented zebrafish. *Vision Res.* **42**, 293–9 (2002).

99. Mumm, J. S. *et al.* In vivo imaging reveals dendritic targeting of laminated afferents by zebrafish retinal ganglion cells. *Neuron* **52**, 609–21 (2006).

100. Schroeder, A. *et al.* The RIN: an RNA integrity number for assigning integrity values to RNA measurements. *BMC Mol. Biol.* **7**, 3 (2006).

101. Reimers, M. & Carey, V. J. [8] Bioconductor: An Open Source Framework for Bioinformatics and Computational Biology. *Methods in Enzymology* (2006) doi:10.1016/S0076-6879(06)11008-3.

102. Diboun, I., Wernisch, L., Orengo, C. A. & Koltzenburg, M. Microarray analysis after RNA amplification can detect pronounced differences in gene expression using limma. *BMC Genomics* (2006) doi:10.1186/1471-2164-7-252.

103. Rainer, J., Sanchez-Cabo, F., Stocker, G., Sturn, A. & Trajanoski, Z. CARMAweb: Comprehensive R- and bioconductor-based web service for microarray data analysis. *Nucleic Acids Res.* (2006) doi:10.1093/nar/gkl038.

104. Hochreiter, S., Clevert, D. A. & Obermayer, K. A new summarization method for affymetrix probe level data. *Bioinformatics* (2006) doi:10.1093/bioinformatics/btl033.

105. Freue, G. V. C. *et al.* MDQC: A new quality assessment method for microarrays based on quality control reports. *Bioinformatics* (2007) doi:10.1093/bioinformatics/btm487.